Blood modelling of diseased vessels inflicted with aneurysm

Shahid Manzoor Toor
Civil and Computational Engineering centre, school of Engineering,
Swansea university, Singleton park, Swansea SA2 8PP.

Thesis submitted to the Swansea university for the degree of
Masters of Science in Computational Mechanics

June 1, 2012

College of Civil Engineering Swansea University

Acknowledgement:

I would like to take this opportunity to thank all those, who supported, encouraged and motivated me in completing my dissertation.

Special thank goes to my supervisor, professor P. Nithiarasu for his patience, excellent guidance, stimulating suggestions, and providing me with an excellent teamwork atmosphere, in carrying out research work.

I would like to pay my deepest gratitude to Dr. Rhodri Beven, who always been there to listen and guide me especially, in using computational codes. I am grateful to Dr Igor Sazonov, who helped me in mesh generations and segmentations. I am also thankful to school of engineering for providing with computational facilities.

Finally, I appreciate financial support provided by European commission.

Abstract

The objective of study is to carry out blood flow modelling in diseased blood vessel inflicted with aneurysm, to develop an association between hemodynamic parameters and atherosclerosis formation. First a detailed review has been presented, describing the current status of aneurysm and available treatment options, along with their associated complications.

In this work to model blood flow through diseased artery, $3\mathbb{D}$ Naiver stoke equations are solved, under the assumption that flow is incompressible, unsteady, Newtonian and pulsatile. In case there is turbulence Sparlart-Allmaras model involving single transport equation is used. For modelling transient flow, temporally varying velocity profile obtained as a numerical solution of Helmholtz equation are prescribed as boundary conditions. The solution scheme employed is characteristic based spilt algorithm in conjunction with artificial compressibility i.e. CBS-AC scheme. The spatial discretization is performed by globally conservative finite element methods. For the solution in-house computational code implemented in Fortran were used on the in-house computing system.

A preliminary test case involving lid-driven cavity flow problem is studied to verify the computational codes. This is followed by a comparative study of a model blood vessel with and without fictitious aneurysm. In case of healthy model artery the flow was found to be smooth, without any localization of hemodynamic parameters. However, the result of inflicted model artery, suggested that at site of aneurysm wall shear stress is significantly lower compared with other sites.

Finally, a patient specific thoracic aortic aneurysm case, is modelled form the Computed Tomographic (CT) scan data. The analysis of patient specific case showed that wall shear stress is lower at the sites, where aneurysm there is aneurysm. However, wall shear stress found to be concentrated at those regions, which were either proximal to the aneurysm or involving bend and kink. These result were supported by a second patient specific case, which showed similar trend of wall shear stress and oscillatory shear index. This work concluded with the observation that wall shear stress can characterise the risk factors associated with the aneurysm.

Contents

List of Figures

List of Tables

Chapter 1

Literature Review

Ahead of publishing as a book chapter

1.1 Arterial aneurysm and its current status

Arterial aneurysm is defined as the portion of an artery, where focal dilation occurs resulting in at least 50% increase of expected normal diameter [29, 24]. The largest artery which comes from the heart and runs down through the chest and abdomen is called the aorta, has been reported to be affected by aneurysm in most of the cases one such case is shown in figure 1.1. Aortic aneurysms have been found in both the chest and abdomen areas, thereby classified into thoracic aortic aneurysm (TAAs) and abdominal aortic aneurysm (AAAs) respectively. However, there is a high prevalence toward the abdomen, supported by the fact that 80% of aortic aneurysm cases are those of AAAs [29]. Arteriosclerosis and weakening of arteries contributed by the factors including male gender, ageing, smoking, family history, hypertension, high blood pressure and atherosclerosis, render patients more susceptible to the increased risk of arterial dilatation [24, 38]. Aneurysm can either be true or pseudo-type. The true aneurysm involves complete arterial wall dilation of diseased section, commonly have fusiform morphology, but can be saccular in some cases; whereas pseoduaneurysm are resulted from arterial tear or dissection of aorta[23].

Unfortunately, majority of the aneurysms grow asymptomatically, and are encountered incidentally during routine clinical test such as ultrasound or X-ray performed to diagnose other diseases [114]. The chances of abdominal aortic aneurysm to be symptomatic are rare, 1 out of 1250 patients can show symptoms such as back pain, sensation of pulsation, abdominal or chest pain [38, 25, 115]. Aneurysm being asymptomatic tends to grow until a rupture or dissection at one or more sites occurs, which is often catastrophic, and carries an overall mortality rate as high as 90%. However for the patients who managed to reach hospital, lower mortality rates $40 - 50\%$ have been reported [62, 96, 115].In contrast to the ruptured cases, mortality rates documented for electively repaired aneurysm stand as high as 10% [115]. One argument to minimize mortality related to rupture is to pass elderly, male population, through scanning or screening trials to find whether affected by the aneurysm and could be repaired electively prior to rupture. Screening studies carried out in the UK have suggested that prevalence of abdominal aneurysm varies 1.3-12% with respect to age group and definition of aneurysm [38].

Aortic aneurysm rupture is ranked as the *thirteenth* commonest cause of death in the Western World. It has been documented that it leads to about $15,000$ deaths each year in the US and about $8,000$ deaths per year in England [18]. The incidence of abdominal aortic aneurysm is higher in the elderly men than in women and young people. A systematic review of a large number of studies has shown that prevalence of AAAs disease is $60 - 90\%$ among the elderly male population [70, 66, 45]

In the earlier studies, diameter has been regarded as a deterministic parameter of prime importance which characterises the risk of aneurysm rupture [142, 87]. The rate of aneurysm rupture is directly related to the aneurysm size [53]. The threshold value, if crossed, height-

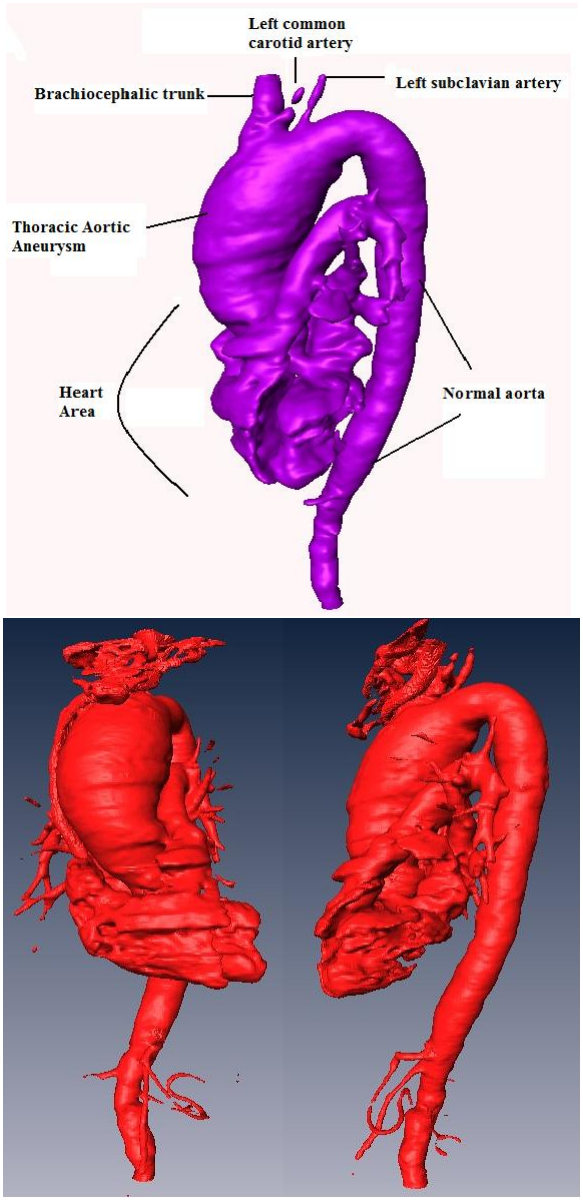

Figure 1.1: Aortic aneurysm, obtained after segmenting CT scans in AMIRA

ens the risk of preoperative rupture. In the case of abdominal aneurysm, this is 5.0-5.5 cm; whereas it is 6.0 cm for thoracic aortic aneurysm [57, 33]. However since last few years, it has become a controversial issue, because about $10-20\%$ of aneurysm ruptures are those which even have not yet crossed the threshold limit [33]. Different studies have evolved to find a true parameter which can predict the risk of aneurysm rupture. Computational fluid dynamics (CFD) analysis based on the finite element discretization has shown that maximum wall stress is a far better indicator, because it combines size of aneurysm with other parameters like blood pressure and geometry as well [64, 34, 49]. For watchful waiting CFD tool could be an ideal option than just relying on the size of aneurysm. Numerous surveillance studies of aneurysm advocate that without treatment freedom from rupture is impossible [10, 38]. Five year survival rates of un-operated aneurysm, reported by investigators are $20-50\%$ depending on association with other atherosclerosis and cardiovascular diseases [88, 114]. Zarins et al.[142] have reported that preoperative aneurysm size also controls the long term result after the treatment. However, it is a common practice to treat aneurysm once it meets the threshold criterion, because delay in repairing causes to enlarge size which leave patients at the increased risk of unfavourable postoperative outcomes [35].

1.2 Techniques used to treat patients:

The risk of rupture can be prevented by repairing the aneurysm with either open surgical repair (OSR) or endovascular aneurysm repair (EVAR). The basic goal behind both of the techniques is exclusion of arterial portion afflicted by aneurysm from luminal pulsatile blood pressure generated by heartbeats and hence excessive wall stress, thereby creating an artificial passage for the blood to flow, by deploying a synthetic conduit. Deployed conduits are called grafts in open repairing approach and stent grafts in case of EVAR.

1.2.1 Brief description of Open repair:

Open surgical repair (OSR) is a traditional standard treatment modality based on a well established procedure to repair aneurysm, its use dates back to early 1950 [56, 53]. It involves a large incision at the site of the aneurysm to access the diseased section of the aorta, thereby clamping it and after removing intraluminal thrombus and calcification, a synthetic graft is sewn to the healthy aortic neck to exclude the aneurysm [120]. Open repairing is a substantial invasive procedure, followed by a large amount of blood and fluid transfusion, long hospital stay and recovery time. Overall mortality rates for elective surgical repaired aneurysm, found in literature range $2-10\%$ [53, 50, 46, 101]. The good results obtained by elective open repair are in contrast to those in the case of emergent repair of ruptured aneurysm, for which reported mortality rates are $28-60\%$ [124, 127, 113, 16, 73, 107]. Despite the fact that open repair is regarded as a good treatment option for the young patients having long term life expectancy, for the patients with ruptured aneurysm, aortic dissection, severe co-morbidities and complications it has limited use because of worse outcomes in terms of peri- and post-procedural mortality and morbidities.

1.2.2 Endovascular aneurysm repair (EVAR):

Surgical repair is difficult to tolerate for aged and co-morbid associated high risk patients and those with ruptured aneurysms. Endovascular aneurysm repair *(EVAR)* has emerged as an alternative treatment option, where major operation can be avoided by deploying an endovascular graft through a remote site. The presentation of this method is controversial; however, this idea has been debated since the late 1960*s*. It has been reported that it was Dotter [76, 80] who first used endoluminal repair in 1969 in an animal trial, whereas the idea of deploying prosthetic graft transfemorally was first presented by Balko et al. [117] in 1986. The first successful report of implanting stent graft endovascularly is credited to J. Parodi [122], who performed the first endoluminal treatment of abdominal aortic aneurysm in 1991 with a custom made stent graft. Whereas, for the patients with ruptured aneurysm, EVAR was first used in 1994.

In the endovascular repair, prosthetic graft supported by a metallic wire-frame called stents, is implanted transfemorally to diseased site with a catheter guided by fluoroscopy and deployed by either balloon or more usually self-expanding mechanism[76]. *EVAR* treatment provides patients with a minimally invasive procedure, significantly reduced perioperative mortality, decreased hospital stay and recovery time. *EVAR* is a useful treatment option, offering good short term results and similar midterm outcomes as the open repair; however, it does not sustain these good early results for the longer period of time [110].

1.2.3 EVAR is a viable treatment option:

EVAR was first developed and used for the patients who were not candidates for *OSR* by any means, therefore to make a comparison special consideration should be paid to their respective selection criterion. However with continuous evolution to date it is the most commonly used technique to repair aortic aneurysm in the US. Currently, $40 - 60\%$ [17, 79] of the patients suffering from the AAAs are treated endovascularly. Since last 30 years from its innovation EVAR has undergone several modifications and improvements in both technology and devices used. The evolution phase can be described through ongoing changes such as: uni-body to modular devices; tube graft to aorto-uni-iliac and to bifurcated devices; suprarenal vs infrarenal fixation; use of barbs and hooks for active fixation; introduction of fenestrated and branched graft, and concept of endofit and Enovus.

To evaluate post-procedural outcomes of EVAR numerous studies have been carried out, and have shown satisfactorily good short and midterm results, some of these studies are outlined in the table 1.1. The early success of EVAR is measured in term of peri-procedural survival rates, absence of technical failure and secondary clinical interventions, and most importantly freedom from rupture. According to reported results peri-operative and 30 days mortality noticed ranges $1.0 - 2.3\%$, technical and clinical success along with freedom from aneurysm rupture can be achieved in majority of the cases. The reported results by different investigators clearly, indicate that EVAR is a feasible alternative treatment option

Reference	EVAR cases	Mean age (y)	Male population (%)	Technical success (%)	Primary clinical success (%)	Freedom from rupture (%)	30 days mortality (%)
Marin et al. [70]	817	74.30	83	93.8	65 ± 8 at 8 years	98 ± 1 at 9 years	2.3
Verhoeven et al.[123]	365	74.0	89	91.0	71 at 3.5 year	92 at 7 years	1.1
Wahlgren et al.[130]	1000	74 ± 7	86				1.8
EVAR trial-1 [45]	543	74.20	91			98	1.7
Wang et al.[133]	192	73.0	88	97.90	78 at 4 years	100 at 6 years	0

Table 1.1: Short term and Midterm EVAR Results

for the patients with suitable anatomy. However, good results of EVAR do not sustain for the patients with unfavourable anatomical features and those already unfit for OSR. The outcomes of EVAR trial-2 [95] conducted in the United Kingdom for the patients to whom, OSR was denied, shows a considerable peri and 30-days mortality rates.

1.3 Contraindications and anatomical restrictions to the liberal use of EVAR:

The primary restrictions to the liberal use of EVAR are unfavourable anatomical and morphological characteristics, mainly related to the proximal aortic neck. The proximal neck for AAAs is defined as part of healthy aorta between the most caudally, located renal artery and beginning of the aneurysm. Hostile behaviour of aortic neck is defined by its size, length, pulsatility, and thrombus and calcification lining [20]. In the most of guidelines limiting value of aneurysm size considered is 5.5cm. The possibility of sideways lateral movement, which is responsible for migration and type-I endoleak, in the larger aneurysm is higher compared with those having smaller dimensions. Post-procedural aortic neck dilatation (AND) is a continuous risk and significantly associated with pre-procedural aortic neck diameter. Cao et al.[12] have reported the outcomes of EVAR trial with 230 patients, they observed aortic neck dilatation in 28% of the patients, where in 77% cases dilation was $3mm - 4mm$ after median follow up of 2 years. The rate of intervention was higher in patients with the AND. Litwinski et al. [67] have found a strong correlation between the aortic neck dilatation, and the migration of devices.

Most of the devices used in endoluminal treatment, requires healthy infrarenal aortic neck of at least $10 - 15mm$ [27, 25] in order to obtain a landing zone and seal, between the endovas-

cular graft and the aortic wall. In the early generations of prosthetic grafts, unfavourable aortic neck length has been found to contraindicate EVAR in 40-50% [94, 2]. The outcomes of several studies have shown that unfavourable neck anatomy is linked to the increased incidence of migration, endoleaks and proximal attachment failure [4, 94]. However, with the ongoing improvement and advent of new branched, fenestrated and suprarenal fixation devices, now short aortic neck length is no more a predominant factor of contraindication [78]. In addition usage of new devices has widened the spectrum of EVAR by making it suitable to the patients with hostile neck, thereby creating more candidates for the EVAR.

The variation in the aortic neck diameter between systolic and diastolic phase is different among individuals; it ranges from 0.9 mm to 2.4 mm [121]. Arko et al.[4] have reported periodic variations in the aortic diameter up to 11% during a cardiac cycle. Moreover, changes in dimensions were observed both along the anterio-posterior (AP) and lateral direction as well. It is always ideal to use dynamic imaging tool to dimension aorta for prosthetic graft. However in case of static imaging tool it may need an oversizing by an appropriate factor.

Several investigators have claimed that neck angulations is one of the prominent factors associated with severe post-procedural complications. With the advent of new flexible devices, maximum treatable aortic neck angle is 60°. The risk of experiencing adverse event after EVAR is directly related to the degree of angulations [109, 27, 51]. However, Goncalveset et al. recently, [40] carried out a study with the endurant stent graft, have obtained satisfactory post-procedure results for the patients with angulated aortic neck.

Aortic neck thrombus and calcification lining in more than 50% circumference contraindicate EVAR. Proximal endoleak and migration have been reported to occur after EVAR, as a result of inadequate seal because of presence of plaque in the neck [27]. Moreover, some investigators are of the opinion that thrombus lining is also responsible for endotension, because it can cause pressure wave to transfer from neck to the aneurysm sac [135]. In contrast to the aortic neck, Sampaio et al.[97] have reported that presence of the thrombus in the aneurismal sac is advantageous because it can occlude the lumbar and mesenteric arteries thereby checking type-II endoleak.

Transfemoral implantation through tortuous, angulated, diseased and too small arteries especially encountered in the women; is often difficult resulting in technical failure of EVAR. Different guidelines have reported that for deploying stent graft without causing any rupture, diameter of common femoral arteries should be at least 7 mm without being tortuous and atherosclerotic [25]. The presence of the branch vessels in the aneurysm sac have been found to be associated with increased risk of type-II endoleak and ischemia of healthy organs. The retrogradations of blood stream in the side branches which is responsible for endoleak is a severe complication, often demands reintervention.

Limiting values of anatomical parameters are listed in the table 1.2, which if crossed patients are not considered as suitable candidates for the EVAR. For the patients satisfying these criterion, once operated good postoperative results are expected. Choke et al.[20] have reported that with the ongoing improvements and increased experience now more and more patients with hostile neck are being offered EVAR. Moreover, they studied hostile group of patients and found that short term results are encouraging use of EVAR.

AAA anatomical parameter	Hostile neck
Aneurysm diameter	$\leq 55mm$
Aneurysm neck diameter	$\leq 28mm$
Infra- renal aortic neck length	$\leq 10mm$
Proximal neck angulation	$\leq 60°$C
Circumferential thrombus lining	$\leq 50\%$
Calcification lining	$\leq 50\%$
Iliac fixation length	$\leq 10mm$
Access vessel diameter	$\leq 7mm$
No. of distal and branch vessels	minimum

Table 1.2: Characteristics of suitable candidate for EVAR

1.4 Design and development of stent grafts:

A stent graft is an artificial flexible blood conduit designed to act as a false lumen at the site of the aneurysm. It consists of a biocompatible graft supported by the foldable metallic stents along its body. In the early generations of endovascular graft, the use of stents was limited to proximal and distal locations only, as was the case in the Parodi's [85] report where stents were used proximally only, to provide with anchorage to the device. However soon after the early deployment, it was realized that in order to provide with columnar strength, avoid compression and kinking, stents should be provided along the entire length of graft [1].

Endoskeleton vs exoskeleton stent pattern: In the commercially available endoluminal prostheses, both endoskeleton (inside) and exoskeleton(outside) stent patterns are used. Fogarty et al.[37] have reported, for the patients with severe angulations endoskeleton profile could lead to abrasion of fabric against the ends of stents, with perforation induced by graft porosity. On the other hand the liberal use of exoskeleton profile leave the patients at the continuously increased risk of vessel injury, could result in thrombus and embolus formation. In an endoluminal prosthesis stents are positioned in three different configurations depending on location: regular stents placed in the middle portion of graft; oversized sealing stents used in the proximal and distal ends to provide with extra radial strength; and oversized bare metal stents used for suprarenal fixation [58].

Selection of stent material: Stent grafts used in aortic aneurysm repair varies in diameter $20-40mm$ and in length $30-60mm$, they need to be compressed into a sheath of $18-24Fr$,

so that can be deployed through restricted dimensions of access arteries. Therefore an ideal material should be flexible and thin, so that it can be folded and simultaneously has high stiffness to bear radial pressure. Most commonly, used material for stents are Nitinol and stainless steel . Nitinol is a shape memory alloy consists of an equiatomic amount of Nickel and Titanium, shape memory effect can be triggered either thermally or mechanically. In most of endovascular prosthesis supported by Nitinol, shape memory effect is achieved mechanical i.e. by superelasticity or changing stress state [54]. In some designs, stents used are manufactured from stainless steel (316L) because it is cheap, easy to fabricate into desired profiles, have high tensile strength and resistant to corrosion. However, in contrast to stainless steel, to date Nitinol stents is preferred choice because of shape memory effect, good flexibility, and their ability to be positioned and followed by magnetic resonance imaging (MRI)[105, 11].

Self-expandable vs balloon expandable stents: There are two distinct classes of stents on the basis of deployment procedure, termed as self expandable and balloon expandable. It is difficult to establish superiority of one over other, nonetheless self expandable stents are easier to implant. Balloon expandable devices are the first commercially available designs, manufactured in the crimped state and expanded by inflating a balloon resulting in plastic deformation of stents. Whereas, self expandable stents are manufactured in a predefined vessel size and then constrained into small size by compressing, so that can be delivered at site by minimal invasive procedure. Self expandable stents are normally made from shape memory alloy, and have properties of super-elasticity, therefore does not have any strength limitations. For an identical design balloon expandable stents are stiffer compared with self expandable, because material (stainless steel) used has a higher modolus of elasticity. Balloon expandable stents have better propereties of apposition to the aortic neck, thereby limiting endoleak and migration [50]. Most commonly used stents in concert with vascular graft are self expandable. It has been reported that self expandable stents are more friendly to adapt the postoperative changes during remodelling of excluded aneurysm. Research is going on to combine the best features of both of these design into one i.e. balloon expandable superelastic stents [28].

*Structural design of stent:*Stents used in endvascular graft are mainly, derivative of the cardiovascular stents in shape and material. The design considerations for both cardiovascular and endovascular stents are similar, including radial strength, flexibility, and its capability to provide with the easier deploying procedure. Stent design is believed to be second strongest factors contributing toward the postprocedural complications, after morphology of vessel. Currently, there are numerous geometrical configurations under use, however, multicellular is the one which combines best possible features of both coil and tubular designs [98, 37, 105, 139]. The comparison of structural properties of different stents designs are outlined in the table 1.3.

Stent grafts are available in both flexible and rigid design. The rigid structure has columnar

Design	Flexibility characteristics	Stiffness	Radial strength
Mesh	Not good	High	strong
Coil	Good	low	weak
Tubular	Not good	high	strong
Multicellular	Good	High	strong

Table 1.3: Comparison of structural properties of stents

strength e.g.Aneurx graft, whereas flexible design e.g.Talent device can adapt anatomical changes during remodelling. After the complete exclusion of aneurysm by EVAR, in the absence of any radial force from bloodstream, during remodelling phase diameter of aneurysm sac decreases, resulting in geometrical changes in anatomy and morphology of diseased area. The best design should adapt these geometrical changes without causing any dislocation between stent and graft, and their modular components. In designing the selection of suitable strut diameter is a critical feature, because it controls both the flexibility and stiffness which are counterparts and should be balanced. In most of the cases diameter of struts for aortic stents is about $0.10mm$ [1].

*Selection of graft material:*The selection of suitable material for the grafts is important, and has been reported to be equally responsible for postoperative complications. The direct complication related to graft material is endoleak resulted from porosity and fatigue failure. The material used for manufacturing graft in both custom made and commercially available devices is either polyethylene terephthalate (PET or Dacron), or expanded Polytetrafluoroethylene (ePTFE), which are biocompatible and have long degradation life. Grafts are usually flexible and can be manufactured in any desired shape with a thickness varies $0.1 - 0.3mm$ [1, 54, 25]. Generally, stent are sewn to the graft by polypropylene suture, however in some new design chemically bondage has been used as well.

Modular vs unibody configuration of stent graft: Stent grafts are available in both modular and unibody configurations. The unibody devices include straight tube and aortouniiliac graft. Because of the extension of abdominal aneurysm to the aortic bifurication, less than 10% of AAA patients are candidates for tube graft. Secondly, the use of straight tube has seen to be responsible for increased incidence of endoleaks. The most widely used stent grafts are bifurcated in modular form [44]; however, in case of uniiliac favourable anatomy, aortouniiliac devices followed by femoro-femoral bypass have proven to be useful [6]. Major advantage of modular devices are, there ability to offer easier deployment because of small sized individual component and to provide with the high degree of dimensional adaptability till the last minute of procedure [1]. *Current markete of stent graft:* Currently, there are number of devices commercially, available approved by American Food and Drug Administration (FDA). Desai et al.[25], Eliason et al.[29] and Kamineni et al.[53] have reported the characteristics of FDA approved devices as listed in the table 1.4. Moreover, they have found that all of the these devices are self expandable and require aortic neck length $\geq 15mm$ except Aneurx for which 10 mm is enough for proximal fixation.

Although stent grafts have evolved through several changes and improvement in geometry

Devices	Configuration	Stent material	Graft Material	Proximal fixation	Available size (mm)
Aneurx	Bifurcated	Nitinol	Woven Polyester	Over-sizing	18-26
Talent	Bifurcated	Nitinol	Polyester	Over-sizing	16-36
Excluder	Bifurcated	Nitinol	PTFE	$Anchors \approx 20mm$	19-26
Powerlink	Unibody	Co-Cr alloy	Woven Polyester	Over-sizing	26
Zenith	Bifurcated	Stainless steel	Polyester	Suprarenal barbs	22-32

Table 1.4: Salient features of FDA approved stent graft used in EVAR

and material, but still no device is categorized as optimum design [11]. One of problem common to all device lies in their compactness, which is not supported because of metallic stents presence. Motivated by this fact Enovus stent graft, which has not yet been commercialised and approved by FDA, has come up with a new design and distinguishing feature to all, where graft can be delivered through small iliac and femoral arteries having dimensions up to $4mm$ followed by the biopolymer stent material, which upon hardening can behave as metal [25].

1.5 Complications associated with EVAR:

The primary aim of endvascular treatment is the exclusion of aneurysm from systemic blood circulation, thereby preventing risk of rupture. Despite of improvements, EVAR still demands continuous lifelong surveillance because of associated post-procedural complications as a result of incomplete exclusion of aneurysm. The rate of experiencing postoperative complications is higher among the patients undergo endoluminal repair, than those of open repair group [45]. In the learning curve of endovascular repair, high mortality rates were observed because of limited use to the high risk patients only, however to date with its widespread applications and established procedure initial mortality rates has dropped down to approximately 3% [119]. Several other complications of minor importance have been found, related to endovascular repair of aneurysm and most often can be resolved with satisfactorily outcomes. However, all researchers have claimed and agreed that major complications dictating success of EVAR are *endoleak* and *migration* [136, 131, 41]. Since these problems have directly, challenged the success of EVAR, and therefore demand special considerations through secondary interventions, which otherwise could lead to the enlargement of aneurysm and hence rupture. According to the outcomes of EVAR trial-1 [45] rate of intervention was 20% among the patients treated endoluminally.

1.5.1 Endoleak:

Endoleak is the most common complication associated with the endovacular repair, defined as persistent blood flow in the area between the outside wall of graft and adjacent vascular segment being treated, called aneurysm sac [136]. In some studies endoleak has been reported as principal failure cause of endovascular procedure, because accumulation of blood in the sac causes to increase endolumnial pressure leading to enlargement of aneurysm and hence rupture. However, other investigators contraindicate this argument on the basis that rupture cases can be seen in the patients with small size of aneurysm [48]. The overall incidence of endoleak have a wide spectrum ranging 10%-50%.

Primary vs secondary Endoleaks: Endoleaks have seen to occur at various stages, however more prevalent during first 30 days after endvascular procedure [26], thereby classified as primary endoleak. Endoleak seen in the early stages could vanish itself in follow up because of thrombus formation and similarly, can appear in long run because of remodelling and device failure. Clouse et al.[22] have identified incidence of endoleak in 52.3% cases at the time of discharge, which does not sustain in long run and noticed to drop down to 30.9% after one year and then remained almost stagnant in the upcoming years i.e. by the end of fourth year it was 30.4%.

Detection of Endoleaks: Three different modalities: ultrasound(US) or sonography; computed tomography(CT); and magnetic resonance imaging (MRI); have been proposed in contrast enhanced mode for detection of endoleak. For early detection CT scan is the best option; however, for surveillance use of the contrast enhanced ultrasound is advantageous as it provides with a method where use of iodinated contrast agent, radiation exposure can be avoided; with a fast, inexpensive, noninvasive and high temporal resolution method [26, 136].

Types of Endoleaks: Endoleaks are classified into five different types on the basis of origin of in flow leakage source and named numerically. *Type I* originate from proximal and distal attachment sites; *type II* as result of retrograde flow in the sac related branch vessels; *type III* from between junctions of modular component and structural failure; *type IV* is reported from graft porosity; and *type V* is defined as pressurization of sac without any evident sources of leakage [26]. Description of different types of perigraft leakage along with possible causes, treatment options and incidence are listed in the table 1.5.

Surveillance and management of Endoleak:

Surveillance of endoleak involves measuring pressure in the aneurysm sac, because it is directly associated with the risk of rupture. The standard and most reliable method to measure intralumenal pressure is by placing a catheter percutaneously through common femoral or iliac artery on the side of contralateral limb. In the absence of endoleak pressure will signifivcantly be lower than systemic pressure whereas it would be of same order if there is any chances of endoleak[136]. Despite this method gives precise and accurate

Endoleak	Definition	Reasons	Treatment options	Average Incidence
Type-I	Blood leaking from either proximal (Ia) or distal (Ib) attachment site of stent graft.	It is usually result of inappropriate case selection or incorrect deployment [48, 51].	Treatment is madatory usually repaired by intervening with cuffs, and extenders [50].	For AAA $\leq 6.5\%$ [51] For TAA $\leq 20\%$ [137]
Type-II	Defined as retrograde or back bleeding of blood through branch vessels into aneurismal sac.	Patent vessels including lumbar and mesenatric arteries are responsible for it (Non graft related).	Has benign behaviour, usually treated by Embolization and late thrombus formation can minimize it as well [97].	$8.0\% - 45\%$ [6]
Type-III	Result from dislocation of modular components and mechanical failure of device material.	Because of insufficient frictional grip between components at junction.	Demands emergency treatment, by additional limbs, redo EVAR, and conversion as a last resort.	$0.7\% - 3.8\%$ [6]
Type-IV	Usually, seen at the initial stages, as a result of permeation through the graft material.	The reason is porosity of thin walled fabric graft.	Requires no treatment, seal off itself within first 30 days of procedure	Initial high incidence
Type-V or Endoten-sion	It is pressurization of aneyursm without any evident sign of leakage.	Thrombus lining and attachment of graft to aortic wall might be responsible for transfering pressure to the sac[135, 50]	Demands surveliance, could be treated by redo or open conversion	$2\% - 5\%$ [48]

Table 1.5: Detailed description of Endoleaks

measurement, it is associated with multiple risk. Post-operatively for measuring pressure through a remote access a new technique has been proposed, where pressure transducer either sewn to graft fabric or kept separate, are implanted at the time of treatment. One such commercially, available device is the EndoSure wireless AAA pressure sensor, this device has a capacitor which uses radio-frequency waves to take pressure reading [6]. Management of endoleak includes balloon dilation of unexpandable stent graft, embolization, additional endvascular procedure with extenders, cuffs or second stent graft deployment, and conversion to open repair. In many cases intervention result into successful exclusion of aneurysm from perigraft leakage; however, until some results are available it is difficult to say that outcomes of repaired endoleak are successful [136].As a treatment options for complications arising in the long run after endovascular repair, conversion to open repair is always considered as a last resort.

1.6 Migration:

Migration is longitudinal displacement of stent graft greater than a predefined *threshold* value in the downward direction, with reference to the most caudally located renal artery (In some studies reference point is superior mesenteric artery) [67, 128]. The *threshold* value for defining migration is taken as $10mm$; however, more strict $5mm$ criterion also used. Migration is usually reported as a result of inadequate proximal fixation, short aortic neck, aneurysm neck dilatation and remodelling of aneurysm sac [115]. Stent graft migration is problem unique to endoluminal repair, because in contrast to open repair stent grafts are not sewn to the aortic neck in the EVAR, hence more prone to migration. Resch et al. have carried out an experimental study, and showed that median force required to dislodge a hand sewn graft is $150N$, whereas it is just $5-25N$ for stent graft used in EVAR depending upon device being used [93].

Passive vs active fixation and incidence of migration: Stent grafts are deployed and provided with apposition to the aortic wall by either passive or active fixation. Passive fixation is the most common fixating mechanism among commercially available design, where device is usually oversized by 10%-20% in diameter to provide with a frictional grip[25]. On the other hand active fixation involves use of suprarenal bare metal stents attached with barbs and hooks, provide with a seal without penetrating into full length of aorta. It has been observed that first generation of stent grafts with passive fixation, suffered from increased risk of positional stability compared with present design. Tonnessen et al. [116] have compared $5mm$ migration freedom, among the patients treated with AneuRx (passive fixation) and Zenith (active fixation) and found 67.4% vs 90.1% respectively at 4 years of follow up. Litwinski et al. [67] observed that incidence of losing positional stability in devices with passive fixation was 15.9% with a migration of $\geq 5mm$. Similarly, Heikkinen et al. [47] have observed 10% incidence of post-implantation movement of $\geq 10mm$ with respect to superior mesenteric artery with a mean follow up of 2 years. Zarin et al. carried out a review of multicentre trial and identified that overall incidence of migration was 19.8% at the 3 years of surveillance [141].
However with current design where number of methods have been proposed to engage proximal and distal aortic neck including: use of barbs and hooks; fenestrated and branched limbs; extended bare metal stents; high columnar strength; bifurcated device; and iliac fixation, high rate of migration is now contraindicated. As documented by Thompson [115] and Won et al. [137] that migration may occur up to 3% of the patients with a mean delay of 18-24 month. The phenomenon of migration is a highly time dependent, in a comparative study it has been reported that at follow up of 1 year in the patients who received Zenith device, there was no migration, whereas, by the end of 4 years 2.4% of the patients have shown migration of at least $10mm$ [116].

Pure migration and correlation with endoleak: Migration is also correlated with type-Ia endoleak, which is primary cause of device failure and rupture [25]. Proximal stent graft

failure should not be judged on the basis of caudal movement of device, because in surveillance it has been observed that pure migration where initial aortic neck length should remained constant throughout follow up, is less likely to occur, rather it is always accompanied by aortic neck dilatation, shortening and elongation. Lintwinski et al. have reported outcomes of a study, where migration occurred, without causing patients to lose proximal fixating zone and hence no failure was observed [67].

*Iliac fixation can inhibit the migration:*The importance of iliac fixation has not been much considered as a contributing factor in developing late migration. Nonetheless, currently, number studies exist, showing that it is also equally important in inhibiting migration. Heikkinen et al. [47] have reported that for devices with columnar support (AneuRx), proximal short aortic neck length can be compensated by achieving proximity to iliac bifurcation at the distal site, in order to obtain freedom from late migration. Benharash et al. [7] have also reported that for the patients in which good iliac fixation achieved with both suprarenal and infrarenal fixating devices, no migration was observed. Waasdrop et al. [128] have carried out a study with the Zeinth device to establish a relationship between fixating length and migration, and found that vast majority of migration were observed in the group having short distal and proximal fixation zone.

Management of migration:

- Oversizing $10\% - 20\%$ to counteract aortic neck dilatation in the follow up [25].
- With the use of branched and fenestrated graft the length of proximal fixation zone can be increased by including suprarenal and hostile neck.
- In addition proximal fixation, device should be fixed at the distal attachment site as well, extending bilaterally, till hypogastric arteries [7, 47].
- A new approach involving endostapling and laparoscopic have been developed to prevent endoleak-1 and migration [118].

1.7 Ruptured endovascular aneurysm repair (REVAR):

Motivated from the consistent use of EVAR in electively treating aortic aneurysm, which has proven to be a feasible alternative with satisfactory short and midterm results, has led experienced units to offer endoluminal repairing to the patients with ruptured cases, subjected to suitable anatomy. The first case where endovascular treatment offered to a patient with ruptured aneurysm was performed in Nottingham in 1994 by deploying a aortouniiliac graft followed by femorofemoral bypass [140]. This case showed the feasibility of EVR for ruptured cases and gave a new hope to the patients of being candidate of a less invasive procedure associated with reduced morbidity and mortality. Since then several endluminal procedure have been performed, reported outcomes indicate that short term mortality rate are promising among patients treated by REVAR [72]. Verhoeven et al. [124]

have compared mortality rate of REVAR with open repair for ruptured abdominal aortic aneurysm, and reported 13.9% vs 28.1% respectively. Harkin et al. [46] have reported that half of the patients suffered from ruptured abdominal aortic aneurysm are offered REVAR, with mortality rates 18% compared with 34% in open repair.

1.8 Conversion to open repair:

Conversion to open repair is always considered as a last option, performed only to the patients in whom endvascular interventions could not resolve graft failure led by persistent blood leakage, migration or structural failure of device, or cause of aneurysm enlargement could not be defined or more importantly rupture occurs after EVAR treatment. The rates of open conversion are rare, and seen both in the early stages and in the long run after Endvascular repair. Primary conversion (PC) involves conversion during first 30 days after the EVAR procedure, generally as result of technical or clinical failure and ischemia of basic organs, whereas secondary conversion (SC) is performed after 30 days, it is usually as a result of rupture or mechanical failure of endograft [74]. In a French multicenter trail with 1588 cases repaired endvascularly registered at 8 different centres, it has been documented that conversion was performed in only 34 i.e. 2.1% of patients, including 14 primary, and 20 secondary conversions [74]. In addition Prinssen et al. have reported rate of conversion up to 2.5% of cases [91]. Moulakakis et al. have reviewed literature from 2002 to 2009 and reported an incidence of primary conversion 1.5% and late conversion up to 1.9% [77]. Both primary and secondary conversion have been found to be associated with significant risk of mortality, reported results stand as high as 28.5% for PC and $0.4\% - 25\%$ for SC [74, 77].

1.9 Fenestrated and branched stent graft:

Majority of aneurysm do not involve critical branch vessels in their development, and therefore can be repaired with satisfactory post procedural outcomes. However, in some case in the presence of critical branch vessels, undermining and repairing with EVAR leads to ischemic complications which usually result into open conversion [21, 74]. The basic criterion for successful endovascular implantation of stent graft include hemostatic seal along with secure and stable attachment site to check migration and endoleak [21]. In 44.0%-49.5% of the AAAs patients, aortic neck length has dimension less than $15mm$ and considered ineligible to EVAR [2, 30]. However, since last few years to address these restrictions new devices with fenestrated and branched stents have been proposed and used, which can keep critical vessel patency and also capable of providing with an option to extend proximal fixation zone to the nondilated aorta [6]. Fenestrated graft are now commercially available in Europe after being approved for CE mark, but still undergoing clinical trials in the United states for FDA approval [78].

Fenestrated stent graft is the one which has small holes along its body, and scallops at the edges in order to accommodate positioning of branch vessels. Fenestrated stent grafts

were the first device developed to deal with hostile neck and patency of branch vessels, where bridging to convert into branched devices usually carried out by using open or covered stents. Fenestrated devices were used to repair both abdominal and thoracic aneurysm; however, because of inadequacy to obtain a durable seal, branched stent grafts have been proposed as an alternative for suprarenal and thoraco-abdominal aortic aneurysm. Branched stent graft can be manufactured in both modular and unibody configurations, however modular is more flexible in dimensional adaptability and easy to deploy [21, 125]. The short and mid term outcomes have been analysed by different researchers. Muhs et al.[78] have reported their experience of treating patients with fenestrated and branched endografts, they found that 30-days mortality rate was 2.4% and all cause mortality up to 13% after median follow-up of about 2 years. They also identified that successful hemostate sealing was achieved in 97.40% of cases and cumulative vessel patency after about 4 years was 92%. For finding outcomes of fenestrated and branched endografts, for the patients suffered from thoraco-abdominal aortic aneurysm (TAAA), Bakoyiannis et al.[5] reviewed English literature available between 2000 to 2009. By statistical analysis of the data, they found that overall mortality was 16.1% with mean follow up of 11.8 months, and identified that technical success was achieved in 94.2% of the cases, among other complications the incidence of renal failure was 5.8%. Their result are encouraging, in the use of EVAR with fenestrated and branched stent grafts as an alternative therapeutic treatment option. Greenberg [42] has reported in a clinical case study that introduction of fenestrated and branched stent graft has led one to believe that almost all patients can now be treated by EVAR, despite of anatomical restrictions.

1.10 Suprarenal vs infrarenal devices:

Excluding the cases repaired with fenestrated and branched stent grafts; currently, up to 55%-61% of the patients suffering from AAAs are treated endoluminally with bifurcated and aortouniiliac endografts [13, 2]. Among postprocedural complications, migration and type-Ia endoleak are largely associated with short proximal aortic neck deployment and aortic neck dilation [141, 67]. It has been reported that suprarenal aortic neck is more stable to postoperative dilatation and resistant to atherosclerosis formation [43], thus is an ideal site for fixation. Suprarenal fixation can provide patients with an alternative landing zone for anchoring and secure attachment, especially to those having adverse anatomical restrictions in term of short and angulated neck, and with severe calcification and thrombus lining and there increasing candidate for EVAR [2]. Suprarenal fixation has widened spectrum of EVAR applications by offering it now up to 70% of patients suffering from AAA [119, 129]. However, implantation of suprarenal stents would more likely, result into crossing of renal arteries by stent struts, thereby raising concerns of renal dysfunction. Numerous investigators have carried out comparative studies of EVAR with sprarenal vs infrarenal fixations, and identified that different patients have faced postprocedral renal dysfunction without any discrimination of type of fixating landing zone. Most importantly, they have reported that suprarenal fixation does not play any role in progression of renal artery stenosis

and acute renal events [65, 84, 63, 129, 19]. Malina et al.[68] have carried out a short trial with a mean follow up of 6 month, after deploying Gianturco Z-stent across renal arteries intentionally, they reported that suprarenal fixation, does not lead any renal complication. It has been observed that suprarenal and infrarenal fixations are not even associated with proximal neck dilatation after EVAR, instead it is governed by morphology and remodelling of aneurysm [89]. However, larger studies with longer postprocedural outcomes are required to correlate suprarenal fixation with incidence of renal complication if there is any.

1.11 Cost effectiveness of EVAR vs Open repair:

The cost of EVAR is defined as cumulative sum of cost associated with first procedure, CT scan surveillance, interventions during follow up and conversion if there is any. For the patients with favourable anatomical and morphological features, EVAR seems to be more cost effective approach, as it offers short term hospital stay, and is associated with less mortality and morbidity rates. However, short term cost benefits do not sustain during the follow up, Prinssen et al.[91] have reported an estimate of EVAR cost, $3631 at the time of implantation, which increased to $9729 at the follow up of 5 years i.e.increase up to 268%, indicating that it is strong function of time. They have also identified that CT scan surveillance contributed up to 65% toward total cost. Similarly, Patel et al. have reported that there is an additional cost of 49.6% associated with EVAR compared with open repair for about 8 years of quality-adjusted life [86]. The commercially available endograft, because of sophisticated manufacturing facilities and modular component production in small lots, also lead EVAR to be an expensive procedure; which is a reason for custom manufacturing of stent graft as well. Fotis et al. [39] have compared short term cost effectiveness of EVAR vs OSR and reported that a major contribution toward the overall cost associated, is from expensive endograft (median cost $24836.50), which according to their results 11.2 time more costly than its counter part graft used in open repair. However a large number of investigators are of the opinion that if late complications do not occur then EVAR is cost effective [86, 91]. A true assessment is impossible until long term results are analysed involving a multicenter trial.

Chapter 2

Flow properties, Hemodynamics parameters and Governing equations

In systemic circulation, blood flows from the heart through largest vessel called aorta, continuously branching into further small arteries, thereby distributing blood to the different organs. The performance of heart is periodic, where simultaneous ejection and refilling of its chambers occurs, supported by the continuous opening and closing action of valves. The repetitive movement of heart is divided into two phases: systolic and diastolic, during the first ventricles contract, followed by relaxation period. A complete cardiac cycle is completed in a duration of about 0.8 *seconds*. The periodic time period varies depending upon the location of arteries in the cardiovascular system. Since flow of blood is periodic and pulsatile, therefore all of the flow variables should be described as having periodic fluctuation.

2.1 Flow properties of blood:

Blood is a biological fluid, consists of about 40% particles in suspension and with remaining volume contributed by plasma. In most of individuals amount of blood is in between 4.5 to 6.0 litres [3, 132]. In general for modelling flow through the diseased blood vessels density, viscosity, hemodynamic pressure, and velocity variations are of major interest and hence will be described briefly.

2.1.1 Density and viscosity of blood:

The density of blood is a strong function of hematocrite, and varies with temperature changes. Blood is slightly heavier compared to that of the water, with reported density ranges $1000 - 1070 Kg/m^3$ [3, 132, 112, 75]. In this study the value of density used is equal to $1000 kg/cm^3$.

Viscosity (μ) is a transport property which offers frictional resistance to the applied shearing force, thereby restricting rate of deformations. The viscosity of blood is regarded as a constant value, which makes it possible to model blood as incompressible fluid. Blood viscosity is measured in $centi - poise(cp)$, where 1000 $cp = 1$ $Pascal.second$. Viscosity of blood is a given as contribution from both plasma and suspended cells. As about $95 - 99\%$ [3, 81] of the particle volume is because of RBC, thus contribution from other particles being too small can be neglected. Hematocrite (Ht) defined as % by volume occupied by the RBC. There are number of approximation exist, relating concentration of hematocrite, however the simplest form is described by the Einstein formula given as:

$$\eta_{blood} = \eta_{plasma}(1 + 2.5Ht) \tag{2.1}$$

Where $\eta_{plasma} = 1.5$ cp and concentration of hematocrite (Ht) varies between $40\% - 50\%$ [81]. According reported results viscosity of blood ranges 3 to 6 cp [3, 132], however in CFD studies usually, $3.5 - 4.0$ cp is assumed. Viscosity of blood is a function of shear rate and varies with respect to the vessel diameter, however this dependence can be neglected for large sized vessels. In this work the value of viscosity used is equal to $4cp$. Blood is a non-Newtonian fluid [81], nonetheless it has been reported that for the larger blood vessels e.g. aorta, viscosity is proportional to the shear rate, and thus can be modelled as Newtonian fluid [112].

2.1.2 Pressure wave form:

Blood pressure is defined as force induced by heart, causing blood to flow through the vessels by overcoming peripheral resistance. The variations of pressure over a cardiac cycle, along with closing and opening position of valves are represented in the figure 2.1. During the systolic phase, left ventricle starts to contract which upon building up a certain pressure level called diastole pressure opens aortic valve, is followed by further contraction causing blood to eject into the aorta, thereby creating highest cyclic pressure called systolic pressure. For a normal individual systolic blood pressure is recorded equal to 120 $mmHg$, whereas diastolic pressure is 80 $mmHg$, with an alternation of 40 $mmHg$ called pulse pressure [102]. Blood pressure measured in the aorta is called aortic pressure, has also been shown in the figure 2.1 with dotted line.

2.1.3 Cardiac output and blood flow rate:

Cardiac output (CO) is defined as amount of blood pumped per minute as a result of ventricles contraction. CO depends on the pulse rate and can be computed by using stroke volume which is amount of blood ejected per heart beat. On average for a resting individual the pulse rate is $60 - 80$ bpm, with a stroke volume ranging $60 - 70$ mL [100], thus approximately cardiac out can be determined as:

$$\text{Cardiac output (CO)} = 70\ bpm \times 70\ mL = 4900\ mL/min. = 4.90\ L/min. \tag{2.2}$$

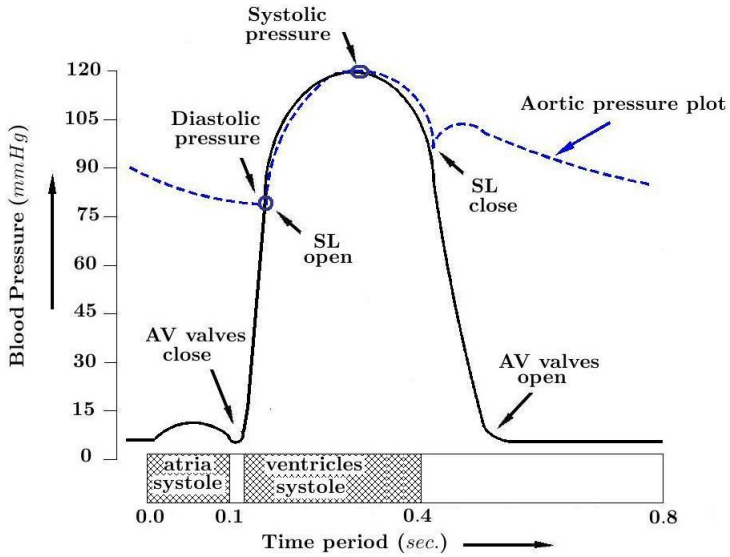

Figure 2.1: Pressure variations over cardiac cycle modified from [102]

However, for a healthy person, cardiac output normally varies $5-6$ $liters/minute$, in this study volume flow rate of blood used is 6.0 L/min..

2.1.4 Velocity variations and turbulence:

The velocity profile of blood in the aorta has fluctuating pattern, because of continuous acceleration and deceleration of blood. The periodic pulsatile behaviour has been reported to be responsible for blood turbulence in the aorta. The variations of Reynold number in the human cardiovascular system are given as [3]: Therefore, for blood flow simulation in

Location	Reynold No.
Aorta	~ 3000
Small veins and arteries	~ 1
Arterioles and micro-vessels	< 1
Capillaries	$\sim 10^{-2}$

Table 2.1: Values of Reynold Number as blood moves away from heart

the aorta turbulence effects should be included.In this study the Reynold number used is 2500, which is usually studied for modelling blood in the thoracic aorta. In general purpose computational fluid dynamic analysis of either thoracic or abdominal aorta, it is assumed that fluid is Newtonian, incompressible and laminar. The most important feature of blood simulation is because of pulsate nature, which not only make it challenging to capture real flow situation, but also demands more computational resources and time.

2.2 Hemodyanamic parameter of interest:

The hemodynamic parameters can characterise the risk associated with the atherogenesis and formation of atherosclerosis inside a blood vessel. Among other parameters wall shear stress found to have more predominant effect. Shear stress is the tangential force caused by the blood flowing through the vessel. Wall shear stress is studied in conjunction with the oscillatory shear index.

2.2.1 Time averaged Wall shear stress (WSS)

The traction vector $\mathbf{t}$ which accounts for the surface forces along a normal direction $\mathbf{n}$ defined as $\mathbf{t} = \sigma\mathbf{n}$, where σ is Cauchy stress tensor. The shear stress can be additively decomposed into normal and tangential components as:

$$\mathbf{t} = \mathbf{t}_n + \mathbf{t}_t$$

where tangential or surface traction component, is given as $\mathbf{t}_t = \mathbf{t} - (\mathbf{t} \,.\mathbf{n})\, \mathbf{n}$. In the transient flow, time averaged quantities are computed to account for mean behaviour. The time averaged wall shear stress:

$$\tau_{tav} = \frac{1}{T} \int_0^T ||\mathbf{t}_t|| dt \tag{2.3}$$

Where T is the time period of cardiac cycle, in this study it is expressed by WSS.

2.2.2 Oscillatory shear index (OSI):

The osilatory shear index used to define transient shear stress regime experience by the neo-intimal layers of an artery. It is given as ratio of absolute shear stress to the mean wall shear stress. The absolute shear stress is defined as magnitude of time-average surface traction vector [52].

$$\tau_{abs} = \left|\left| \frac{1}{T} \int_0^T \mathbf{t}_t dt \right|\right|$$

OSI can be expressed as:

$$OSI = \frac{1}{2}\left(1 - \frac{\tau_{mean}}{\tau_{abs}}\right) \tag{2.4}$$

Thus OSI always lies in the range $[0, 0.5]$, the value of OSI equal to zero corresponds to no cyclic variation and value equal to 0.5 represents reverse flow. Since OSI only account for direction of wall shear stress not magnitude, therefore it quantifies the time during which flow recirculate and does not follow the predominant flow direction.

2.3 Navier stoke equations for blood flow modelling:

Analysis of fluid problems, involves basic conservation principles for modelling their flow behaviour. The resulting equations thus obtained are in general called as Naiver stoke equations. In the blood modelling since temperature does not enter as a variable in the equation of state, and often analysis is carried out for pressure and velocity, which can be studied with mass and momentum conservation equations alone. As blood flow modelling is studied under the assumption that flow is incompressible, for which conservation of mass appears as kinematic constraints. Since continuity equation is just a kinematic constraint to the momentum equation, leaving behind 3 momentum equations with 4 (u_1, u_2, u_3, p) unknowns in $3\mathbb{D}$. Therefore, a special algorithm is needed to solve these equations by establishing a linkage between the governing equations, in this study artificial compressibility method has been employed to dealt with this situation.

In artificial compressibility method, a fictitious transient term is added to the incompressible flow field, allowing it to behave as compressible, so that can be solved by widely accepted semi-implicit solution schemes developed for compressible flows. This algorithm is widely used for the steady state solution and is more efficient compared with methods use pressure poisson equation to conserve continuity constraint [60]. Thus, incompressible Naiver stoke equations in conjunction with artificial compressibility scheme can be written as:

$$\frac{1}{\beta^2}\frac{\partial p}{\partial t} + \frac{\partial U_i}{\partial x_i} = 0 \tag{2.5}$$

$$\frac{\partial U_i}{\partial t} + \frac{\partial}{\partial x_j}(u_j U_i) = \frac{\partial \tau_{ij}}{\partial x_j} - \frac{\partial p}{\partial x_i} \tag{2.6}$$

where $U_i = \rho u_i$ is the mass flux and τ_{ij} is given by constitutive relation

$$\tau_{ij} = \mu\left(\frac{\partial u_i}{\partial x_j} + \frac{\partial u_j}{\partial x_i} - \delta_{ij}\frac{2}{3}\frac{\partial u_k}{\partial x_k}\right) \tag{2.7}$$

and δ_{ij} is Kronecker delta. The fictitious parameter β has dimension of velocity, usually termed as artificial or pseudo compressibility parameter. For truly incompressible flow the speed of sound is very high, causing waves to propagate instantaneously, without providing any means for pressure to distribute. However, unsteady fictitious term, creating a phase lag between flow disturbances and their effects on pressure field. The value of β used, should be as high as algorithm employed for the discretization allows, because a small value could cause pressure wave to interfere with the development of viscous boundary layer and hence raises convergence issues [61].

2.3.1 Non dimensional form of incompressible Naiver stoke equation:

For non-dimensional form it is convenient to implement computational code, as it allows to control flow behaviour by a few non-dimensional parameters. There are different scales

employed depending on the problem in hand. In this study following are used:

$$x^* = \frac{x_i}{L}; \quad t^* = \frac{t}{t_\infty}; \quad u_i^* = \frac{u_i}{u_\infty}; \quad \rho^* = \frac{\rho}{\rho_\infty}; \quad p^* = \frac{p}{\rho_\infty u_\infty^2}$$

Where L correspond to the length scale, and variables with subscript ∞ are free stream values of the quantities. The resulting non-dimensional form is expressed as:

$$\frac{1}{\beta^{*2}}\frac{\partial p^*}{\partial t^*} + \frac{\partial U_i^*}{\partial x_i^*} = 0 \tag{2.8}$$

$$\frac{\partial U_i^*}{\partial t^*} + \frac{\partial}{\partial x_j^*}(u_j^* U_i^*) = \frac{1}{Re}\frac{\partial \tau_{ij}^*}{\partial x_j^*} - \frac{\partial p^*}{\partial x_i^*} \tag{2.9}$$

Re is the Reynold number defined as ratio of inertial to viscous forces,

$$Re = \frac{u_\infty L}{\nu_\infty} \qquad \because \nu_\infty = \frac{\mu_\infty}{\rho_\infty}$$

where ν_∞ is the free stream kinematic viscosity. Similarly, constitutive relation for shear stress τ_{ij} in non-dimensional form is given as:

$$\tau_{ij}^* = \mu^* \left(\frac{\partial u_i^*}{\partial x_j^*} + \frac{\partial u_j^*}{\partial x_i^*} - \delta_{ij}\frac{2}{3}\frac{\partial u_k^*}{\partial x_k^*} \right) \tag{2.10}$$

In this study the free-stream values found to be convenient to work with are

$$\boxed{L = 3,\ \mu_\infty = 4 \times 10^{-2},\ u_\infty = u_{meanpeak},\ \rho_\infty = 1}$$

where $u_{meanpeak}$ is the peak mean velocity obtained from pulsatile velocity flow profile. Now onward in flow modelling, non-dimensional form of Naiver stoke equations will be used, however $*$ symbol would be discarded for convenience.

2.4 Turbulence, Reynold averaged Naiver stoke equations (RANS) and Spalart–Allmaras turbulence model:

Under normal physiology blood flowing through the ascending aorta can behave as turbulent only at peak flow situations, however for the diseased patients turbulence have been reported to occurs throughout the cardiac cycle [59, 108]. The presence of bifurcation and arch in the aorta further heighten the risk of flow instabilities, thereby emphasizing need to consider turbulence while modelling. Most commonly, used traditional approach to model turbulence is to use RANS, where a flow property is decomposed into a mean steady value, superimposed by the fluctuations counted statistically. The reason behind its extensive use, lies in the fact that computational resources required for achieving desired accurate solution are modest [126].

In order to write RANS equations for modelling incompressible turbulent flow field, velocity and pressure are first decomposed as: The decomposition follows:

$$u_i = \overline{u}_i + u_i' \quad \text{and} \quad p = \overline{p} + p'$$

Now by time averaging, non-dimensional Naiver Stoke equations are written as:

$$\frac{1}{\beta^2}\frac{\partial \overline{p}}{\partial t} + \frac{\partial \overline{U_i}}{\partial x_i} = 0 \tag{2.11}$$

Similarly, taking mean of momentum equation 2.9, decomposing each flow variable, and after simplifying, resulting time averaged momentum equation is expressed as:

$$\frac{\partial \overline{U}_i}{\partial t} + \frac{\partial (\overline{u}_j \overline{U}_i)}{\partial x_j} = \frac{\partial}{\partial x_j}(\overline{\tau}_{ij} + \overline{\tau}_{ij}^R) - \frac{\partial \overline{p}}{\partial x_i} \tag{2.12}$$

In the time averaged momentum equation a new term ($\overline{\tau}_{ij}^R = -\overline{u_j' U_i'}$) appears as a result of time averaging, is called Reynold stress,and given by the *Boussinesq assumption* as:

$$\overline{\tau}_{ij}^R = -\overline{u_j' U_i'} = \mu_\tau \left(\frac{\partial \overline{u}_i}{\partial x_j} + \frac{\partial \overline{u}_j}{\partial x_i} - \delta_{ij}\frac{2}{3}\frac{\partial \overline{u}_k}{\partial x_k} \right) - \frac{2}{3}\rho\kappa\delta_{ij} \tag{2.13}$$

Where μ_τ is turbulent eddy dynamic viscosity, and κ is turbulent eddy kinetic energy taken as zero i.e. $\kappa = 0$ in this work. Thus by employing constitutive relation the total shear terms can be written as:

$$\overline{\tau}_{ij} + \overline{\tau}_{ij}^R = \frac{(1+\nu_\tau)}{Re}\left(\frac{\partial \overline{u}_i}{\partial x_j} + \frac{\partial \overline{u}_j}{\partial x_i} - \delta_{ij}\frac{2}{3}\frac{\partial \overline{u}_k}{\partial x_k} \right) \tag{2.14}$$

However, system of equations is not yet fully closed, as term turbulent kinematic viscosity ν_τ is undefined, and in this is obtained from the Sparlart Allmaras turbulence models.

2.4.1 Spalart–Allmaras turbulence model:

Spalart–Allmaras turbulence model uses a single transport equation in concert with some constants, to define kinematic eddy viscosity parameter for modelling turbulence [126, 145]. The turbulent dynamic viscosity is related to the kinematic eddy viscosity parameter by

$$\mu_\tau = \rho\widetilde{\nu} f_{v1}$$

The effective transport equation for $\widetilde{\nu}$ is given as:

$$\frac{\partial \widetilde{\nu}}{\partial t} + \frac{\partial (\widetilde{\nu} u_i)}{\partial x_i} = \frac{1}{\sigma_{\widetilde{\nu}}}\left[\left(\frac{\partial}{\partial x_i}(\nu + \widetilde{\nu})\frac{\partial \widetilde{\nu}}{\partial x_i} \right) + C_{b2}\left(\frac{\partial \widetilde{\nu}}{\partial x_i} \right)^2 \right] + C_{b1}\widetilde{\nu}\widetilde{\Omega} - C_{w1} f_w \left(\frac{\widetilde{\nu}}{\kappa y} \right)^2 \tag{2.15}$$

As transport equation has to be used in conjunction with Reynold averaged Naiver stoke equations, which are in non-dimensional form, therefore for consistency, is presented in non-dimensional form. By introducing same scales as used for Naiver stoke equations, with an additional scale given as:

$$\widetilde{\nu^*} = \frac{\widetilde{\nu}}{\widetilde{\nu}_\infty}$$

resulting non-dimensional form as follows:

$$\frac{\partial \widetilde{\nu^*}}{\partial t^*} + \frac{\partial (\widetilde{\nu^*} u_i^*)}{\partial x_i^*} = \frac{1}{Re\sigma_{\widetilde{\nu}}} \left[\left(\frac{\partial}{\partial x_i^*}(1+\widetilde{\nu^*}) \frac{\partial \widetilde{\nu^*}}{\partial x_i^*} \right) + C_{b2} \left(\frac{\partial \widetilde{\nu^*}}{\partial x_i^*} \right)^2 \right] + C_{b1} \widetilde{\nu^*} \widetilde{\Omega} - \frac{C_{w1} f_w}{Re} \left(\frac{\widetilde{\nu^*}}{\kappa y^*} \right)^2 \tag{2.16}$$

Where Re is the Reynold number, all other parameters and constants appearing in the above equation have been defined in the appendix A.1.

The flow behaviour of blood in the aorta is modelled by incompressible Naiver stoke equations, where turbulence is characterised by Reynold averaged approximation, supported by the Sparlart-Allmaras model. For this study flow equations are used in the non-dimensional form, thereby dropping asterisk notations for convenience. In computational fluid dynamics (CFD) study once the flow field is defined, it need to be discretized throughout the domain. The discretization procedure involves both spatial and temporal discretizations depending upon the terms appearing in the modelling equations, as explored in following chapter.

Chapter 3

Discretization, Stability control parameters and boundary conditions

To investigate the behaviour of a flow field, it requires to subdivide whole domain into finite set of small individual components called elements, the behaviour of which can be modelled easily, then by joining up these regions original problem is rebuilt to analyse whole system. The process of decomposing domain into elements is called discretization, usually governed by either of finite volume or finite element procedures. In the current work finite element method has been employed, where conservation principles are satisfied globally.

Most of the fluid problems because of their inability to be expressed in variational form, are solved by Galerkin formulation [36], which is an optimal choice of discretization for the self-adjoint form of equations only [138]. Therefore, governing equation first should be transformed into self-adjoint form. The problem in hand is transient, can exhibit wave nature behaviour, which permits the use characteristic Galerkin procedure, a method which is not only easy to implement but also results into self-adjoint form.

3.1 Temporal Discretization

3.1.1 Characteristics Galerkin method to the incompressible Naiver stoke equations:

Unsteady problems,require both temporal and spatial discretization, where space and time can be linked through characteristics, the representation of one can easily deteriorate other if special consideration is not paid. The temporal discretization of the problem in hand, has been carried by the procedure described by [144]. The temporal discretization of momentum

equation by characteristic Galerkin method results into following expression:

$$U_i^{n+1} - U_i^n = -\Delta t \left[\frac{\partial(u_j U_i)}{\partial x_j} - \frac{1}{Re}\frac{\partial \tau_{ij}}{\partial x_j}\right]^n - \Delta t \frac{\partial p^{n+\theta_2}}{\partial x_i} + \frac{\Delta t^2}{2} u_k^n \frac{\partial}{\partial x_k}\left[\frac{\partial(u_j U_i)}{\partial x_j} - \frac{1}{Re}\frac{\partial \tau_{ij}}{\partial x_j}\right]^n + \frac{\Delta t^2}{2} u_k^n \frac{\partial}{\partial x_k}\left(\frac{\partial p^{n+\theta_2}}{\partial x_i}\right) \tag{3.1}$$

where

$$\begin{aligned} \frac{\partial p^{n+\theta_2}}{\partial x_i} &= (1-\theta_2)\frac{\partial p^n}{\partial x_i} + \theta_2 \frac{\partial p^n}{\partial x_i} \\ or\ \frac{\partial p^{n+\theta_2}}{\partial x_i} &= \frac{\partial p^n}{\partial x_i} + \theta_2 \frac{\partial \Delta p}{\partial x_i} \quad \text{with} \quad \Delta p = p^{n+1} - p^n \end{aligned} \tag{3.2}$$

Similarly, the mass conservation equation in conjunction with artificial compressibility parameter is discretized as:

$$\Delta p = -\Delta t \beta^2 \left(\frac{\partial U_i^{n+\theta_1}}{\partial x_i}\right) \tag{3.3}$$

where

$$\frac{\partial U_i^{n+\theta_1}}{\partial x_i} = \frac{\partial U_i^n}{\partial x_i} + \theta_1 \frac{\partial \Delta U_i^{n+1}}{\partial x_i} \quad \text{with} \quad \Delta U_i^{n+1} = U_i^{n+1} - U_i^n$$

These temporally, discretized equations will provide with the base for using split algorithm, will be described in following section.

3.1.2 Characteristic based split (CBS) algorithm:

In the solution of the incompressible Naiver stoke equations a problem usually encountered, is the presence of zero diagonal terms which render matrix solution impossible. However, it has been suggested that zero diagonal terms can be eliminated naturally, if split algorithm is implemented [71]. It involves splitting of momentum equation, described through following three steps:

Computing intermediate velocity field: Intermediated velocity field is first computed by neglecting pressure terms from the momentum equations, i.e., velocity field can be split into two part written as:

$$\Delta U_i^{n+1} = \Delta U_i^{inter} + \Delta U_i^* \tag{3.4}$$

The intermediate velocity field can be given, by eliminating pressure terms from the equation 3.1, as:

$$\Delta U_i^{inter} = -\Delta t \left[\frac{\partial(u_j U_i)}{\partial x_j} - \frac{1}{Re}\frac{\partial \tau_{ij}}{\partial x_j}\right]^n + \frac{\Delta t^2}{2} u_k^n \frac{\partial}{\partial x_k}\left(\frac{\partial(u_j U_i)}{\partial x_j}\right)^n \tag{3.5}$$

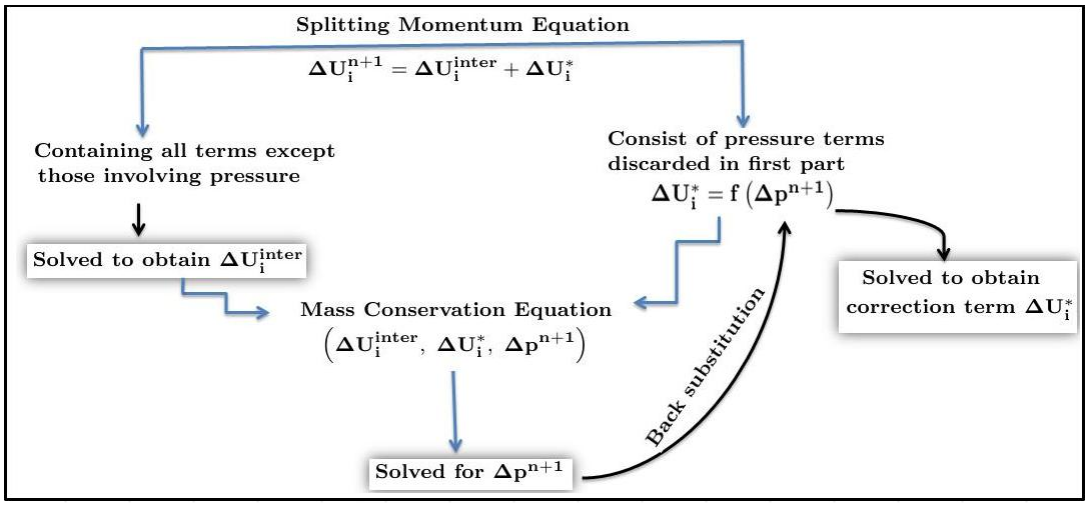

Figure 3.1: Explanation how characteristic based split algorithm works

and correction term (ΔU_i^*) is obtained by comparing 3.5 with 3.1, in term of discarded quantities written as:

$$\Delta U_i^* = -\Delta t \left(\frac{\partial p^n}{\partial x_i} + \theta_2 \frac{\partial \Delta p}{\partial x_i} \right) + \frac{\Delta t^2}{2} u_k \frac{\partial}{\partial x_k} \left(\frac{\partial p^n}{\partial x_i} + \theta_2 \frac{\partial \Delta p}{\partial x_i} \right) \tag{3.6}$$

However, above expression clearly indicates that in order to compute velocity correction term, first pressure Δp need to be computed.

Pressure field calculation: Fro computing pressure field a poisson equation is developed, obtained from the equation 3.3, after substituting velocity field from equations 3.6 and 3.5 written as:

$$\Delta p = -\Delta t \beta^2 \left[\frac{\partial U_i^n}{\partial x_i} + \theta_1 \left(\frac{\partial \Delta U_i^{inter}}{\partial x_i} - \Delta t \left(\frac{\partial^2 p^n}{\partial x_i \partial x_i} + \theta_2 \frac{\partial^2 \Delta p}{\partial x_i \partial x_i} \right) \right) \right] \tag{3.7}$$

The expression obtained for pressure field is self-adjoint, and can be solved for Δp. Once the updated pressure is known then it is possible to compute velocity correction field by employing equation 3.6. The spilt algorithm has been illustrated in the figure 3.1. The system of equations obtained, can be solved in any of explicit, semi-implicit or implicit form, based on the selection of θ_1 and θ_2 values, have been described in section 3.4.1.

3.2 Spatial Discretization:

The use of characteristic based split algorithm results into a system of equations which are self-adjoint [138], thereby making it possible to use standard Galerkin method as an optimal choice for spatial discretization. The spatial discretization is carried out by first

writing week formulation, followed by standard Galerkin procedure, where variables are approximated by shape functions similar to those of weighting functions.

Spatial discretization of intermediate momentum equation: The week formulation of intermediate momentum equation 3.5, after multiplying with w as a weighting function and integrating over domain Ω of problem, where selective use of *Green-Gauss* theorems result into following expression:

$$\int_{\Omega} w\Delta U_i^{inter} d\Omega = -\Delta t \int_{\Omega} w\frac{\partial(u_j U_i)}{\partial x_j} d\Omega + \frac{\Delta t}{Re}\left[-\int_{\Omega}\frac{\partial w}{\partial x_j}\tau_{ij} d\Omega + \int_{\Gamma} w n_j \tau_{ij}^n d\Gamma\right] + \frac{\Delta t^2}{2}\left[-\int_{\Omega}\frac{\partial w}{\partial x_k}\left(u_k\frac{\partial(u_j U_i)}{\partial x_j}\right)^n d\Omega + \int_{\Gamma}\underbrace{w n_k\left(u_k\frac{\partial(u_j U_i)}{\partial x_j}\right)^n}_{Residual\ at\ boundary\ is\ neglected} d\Gamma\right] \tag{3.8}$$

In the above expression n_j and n_k are unit normal vectors introduced by the application of *Gauss* theorem, representing the direction of face fluxes, replaced by their respective nodal values. Now employing standard Galerkin procedure with following approximations:

$$U_i = \mathbf{N}_u\widetilde{\mathbf{U}}_i;\quad u_j = \mathbf{N}_u\widetilde{\mathbf{u}}_j;\quad \Delta U_i^{inter} = \mathbf{N}_u\Delta\widetilde{\mathbf{U}}_i^{inter};\quad p = \mathbf{N}_p\widetilde{\mathbf{p}};\quad \Delta p = \mathbf{N}_p\Delta\widetilde{\mathbf{p}}; \tag{3.9}$$

and using constitutive relationship for deviatoric stress (τ_{ij}) defined by equation 2.7, the fully discretised form of intermediate momentum equation is given as:

$$\int_{\Omega}\mathbf{N}_u^T\mathbf{N}_u\Delta\widetilde{\mathbf{U}}_i^{inter} d\Omega = -\Delta t\left[\int_{\Omega}\mathbf{N}_u^T\left(\frac{\partial}{\partial\mathbf{x}_j}(\widetilde{\mathbf{u}}_j\mathbf{N}_u)\widetilde{\mathbf{U}}_i\right)^n\right] + \frac{\Delta t}{Re}\left[-\int_{\Omega}\frac{\partial\mathbf{N}_u^T}{\partial\mathbf{x}_j}\left(\frac{\partial\mathbf{N}_u}{\partial\mathbf{x}_j}\{\widetilde{\mathbf{u}}_i\}^n + \frac{\partial\mathbf{N}_u}{\partial\mathbf{x}_i}\{\widetilde{\mathbf{u}}_j\}^n - \frac{2}{3}\delta_{ij}\frac{\partial\mathbf{N}_u}{\partial\mathbf{x}_k}\{\widetilde{\mathbf{u}}_k\}^n\right) d\Omega + \int_{\Gamma}\mathbf{N}_u^T\mathbf{t}^d d\Gamma\right] - \frac{\Delta t^2}{2}\left[\int_{\Omega}\frac{\partial}{\partial\mathbf{x}_k}(\mathbf{N}_u^T\mathbf{u}_k)\frac{\partial}{\partial\mathbf{x}_j}(\mathbf{N}_u\widetilde{\mathbf{u}}_j)\widetilde{\mathbf{U}}_i^n d\Omega\right] \tag{3.10}$$

To represent in concise form matrix notation is employed such that:

$$\Delta\tilde{\mathbf{U}}^{inter} = -\mathbf{M}_u^{-1}\Delta t\left[\left(\mathbf{C}_u\widetilde{\mathbf{U}} + \mathbf{K}_\tau\tilde{\mathbf{u}} - \mathbf{f}\right) - \Delta t(\mathbf{K}_u\tilde{\mathbf{U}})\right] \tag{3.11}$$

Spatial descritization of pressure and velocity correction equations: By following same procedure, fully discrete form of both pressure and velocity correction equations, are presented respectively, in matrix form as:

$$(\mathbf{M}_p + \Delta t^2\beta^2\theta_1\theta_2\mathbf{H})\Delta\tilde{\mathbf{p}}^{\mathbf{n+1}} = \Delta t\beta^2\left[\mathbf{G}\tilde{\mathbf{U}}_n + \theta_1\mathbf{G}\Delta\tilde{\mathbf{U}}^{\mathbf{inter}} - \Delta t\theta_1\mathbf{H}\tilde{\mathbf{p}}^{\mathbf{n}} - \Delta t\mathbf{f}_p\right] \tag{3.12}$$

and

$$\mathbf{\Delta\tilde{U}} = \mathbf{\Delta\tilde{U}^{inter}} - \mathbf{M_u^{-1}}\Delta t\left[\mathbf{G}^T(\mathbf{\tilde{p}^n} + \theta_2\mathbf{\Delta\tilde{p}^{n+1}}) + \Delta t\mathbf{L}(\mathbf{\tilde{p}^n} + \theta_2\mathbf{\Delta\tilde{p}^{n+1}})\right] \tag{3.13}$$

where matrices used in the above expressions have been described in the appendix A.2.

3.3 Discretization of Spalart Allmaras Transport equation:

The transport equation used, involves both spatial and transient terms, therefore demands both temporal and spatial discretizations.

Temporal discretization:

The temporal discretization is carried out by characteristics Galerkin procedure, which when applied to the transport equation 2.15, results into following temporally, semi-discretized equation:

$$\frac{\Delta\tilde{\nu}}{\Delta t} = \left[-\frac{\partial(\widetilde{\nu}u_i)}{\partial x_i} + \frac{1}{Re\sigma_{\widetilde{\nu}}}\left(\frac{\partial}{\partial x_i}(1+\widetilde{\nu})\frac{\partial\widetilde{\nu}}{\partial x_i} + C_{b2}\left(\frac{\partial\widetilde{\nu}}{\partial x_i}\right)^2\right) + C_{b1}\widetilde{\nu}\widetilde{\Omega} - \frac{C_{w1}f_w}{Re}\left(\frac{\widetilde{\nu}}{\kappa y}\right)^2\right]$$
$$-\frac{\Delta t}{2}u_j\frac{\partial}{\partial x_j}\left[-\frac{\partial(\widetilde{\nu}u_i)}{\partial x_i} + \frac{1}{Re\sigma_{\widetilde{\nu}}}\left(\frac{\partial}{\partial x_i}(1+\widetilde{\nu})\frac{\partial\widetilde{\nu}}{\partial x_i} + C_{b2}\left(\frac{\partial\widetilde{\nu}}{\partial x_i}\right)^2\right) + C_{b1}\widetilde{\nu}\widetilde{\Omega} - \frac{C_{w1}f_w}{Re}\left(\frac{\widetilde{\nu}}{\kappa y}\right)^2\right] \tag{3.14}$$

Spatial Discretization:

After the temporal discretization is done, spatial discetization is followed by standard Galerkin method by using approximations: $\tilde{\nu} = \mathbf{N}_\nu\hat{\nu}$ and $u = \mathbf{N}_u\hat{\mathbf{u}}$. The corresponding week formulation, along with matrices notation has been presented in the appendix A.3, which results into concise matrix representation as follows:

$$\Delta\hat{\nu} = \mathbf{M_\nu^{-1}}\Delta t\left[(\mathbf{C}_{\nu_1} + \mathbf{K}_{\nu_1} + \mathbf{f}_{\nu_1}) + \frac{\Delta t}{2}(\mathbf{K}_{\nu_2} + \mathbf{f}_{\nu_2})\right] \tag{3.15}$$

Flow equations 3.11, 3.12,3.13 and 3.15, given in matrices notation have been fully discretised both with respect to time and space coordinates and can be solved by making suitable choice for β and Δt, will be explored in the following section.

3.4 Stability control parameters:

After carrying out spatial and temporal descritization of flow equations, there are a few terms still need to discussed before proceeding toward the solution stage, this includes selection of suitable time step (Δt) and artificial compressibility parameter (β). These parameters are interrelated with each other in controlling stability of algorithm employed, and can be discussed for laminar and turbulent flows separately.

3.4.1 Laminar flow, and artificial compressibility parameter (β) and local time step(Δt):

Laminar flow in contrast to the turbulent is a stable flow, modelling of which requires, the use of Naiver stoke equations without transport equation. The solution algorithm used in this work is based on the CBS-AC scheme, where both θ_1 and $\theta_2 \in [0, 1]$ have been used, thus resulting system of equations is conditionally stable with allowable time step should be less than critical value i.e. $\Delta t \leq \Delta t_{critical}$ [145, 82]. Artificial compressibility parameter (β) can either be assumed as a constant throughout the problem domain, or locally defined by accounting convection and diffusion effects. However, second approach has been reported as a recommended choice [145, 82], since it not only provides with a choice for analysing flow at different Reynold numbers, but also allows at a particular Reynold number, to account for convection and diffusion dominated flow regimes. Artificial compressibility parameter (β) can be defined locally as:

$$\beta = \max(\epsilon, u_{conv}, u_{diff}) \tag{3.16}$$

Where ϵ is a small non zero constant , such that β does not approach to zero in any case, in this work $\epsilon \in [0.1, 0.50]$ is used. However, for better results the preferable choice of β should be based on either of convection or diffusion velocities. Where convection velocity (u_{conv}), computed as magnitude of maximum value at a node i for an element as:

$$u_{conv} = |\mathbf{u}| = \sqrt{\max(u_i u_i)} \quad i = 1, 2, ..., N \tag{3.17}$$

The diffusion velocity which defines the relative significance of inertial to viscous effects is given in term of element size(h), and Reynold number (Re) by following expression:

$$u_{diff} = \frac{2}{hRe} \tag{3.18}$$

As value of artificially compressibility parameter is defined locally, thus local time stepping will be introduced as part of computation [82]. The local time step is selected as minimum value between either of convection or diffusion step size.

$$\Delta t_{local} = \min\left(\Delta t_{conv}, \Delta t_{diff}\right) \tag{3.19}$$

where

$$\Delta t_{conv} = \frac{h}{u_{conv} + \beta} \tag{3.20}$$

and

$$\Delta t_{diff} = \frac{h^2 Re}{2} \tag{3.21}$$

In order to keep local time step below critical value and control the convergence rate of solution depending upon problem in hand, usually a parameter called safety factor (SF) is tuned, where true final time step size is given as:

$$\Delta t_{true} = \Delta t_{local} \times SF \tag{3.22}$$

Safety factor used in this study ranges $0 < SF \leq 0.5$.

3.4.2 Turbulent flow and solution parameters:

In case of turbulent flow, fictitious parameter β should include turbulence effects as well.

$$\beta = \max(\epsilon, u_{conv}, u_{diff}, u_{turb}) \tag{3.23}$$

Where u_{turb} is a new term called turbulence velocity, specific to the turbulent flow field, can be defined from equation 3.15 by performing dimensional analysis, as:

$$u_{turb} = \max\left(\frac{1+\hat{\nu}}{Re\sigma_{\hat{\nu}}},\ \frac{C_{b_2}\{\hat{\nu}\}}{Re\sigma_{\hat{\nu}}},\ \frac{C_{w_1}f_w h^2}{Re\hat{\nu}}\left\{\frac{\hat{\nu}}{ky}\right\}^2,\ C_{b_1}\hat{\Omega}h^2\right) \times \frac{1}{h} \tag{3.24}$$

Since turbulence is the property of flow field, its effect can be introduced via the definition of convection time step given in equation 3.19, where a change in the value of β would automatically update size of local time step.

3.5 Recovering transient solution and dual time stepping:

For the problem in hand CBS-AC algorithm has been employed, where in order to recover transient solution, a time dependent term is added into the momentum equation either at step-1 or step-3. The introduction of transient term splits domain into several local steady states [82], where for each real time step an iterative pseudo algorithm is applied to obtain divergence free solution up at local level. In this study time dependant term is added into step-3, where corresponding updated equation is given as:

$$\boldsymbol{\Delta\tilde{\mathbf{U}}} = \boldsymbol{\Delta\tilde{\mathbf{U}}}^{\mathbf{inter}} - \mathbf{M_u^{-1}}\Delta t\left[\mathbf{G}^T(\tilde{\mathbf{p}}^{\mathbf{n}} + \theta_2\boldsymbol{\Delta}\tilde{\mathbf{p}}^{\mathbf{n+1}}) + \Delta t\mathbf{L}(\tilde{\mathbf{p}}^{\mathbf{n}} + \theta_2\boldsymbol{\Delta}\tilde{\mathbf{p}}^{\mathbf{n+1}}) + \underbrace{\frac{\Delta U_i}{\Delta\tau}}\right] \tag{3.25}$$

$\Delta\tau$ is physical time step, choice of which is dictated by the solution accuracy, instead of numerical scheme stability, therefore has no restriction on the pseudo time step. Transient velocity is approximated by backward differencing formula (BDF), order of approximations can effect the solution accuracy. In the current study third order differencing formula $BDF3$ has been used given as:

$$\Delta U_i = \frac{11\Delta U_i^n - 18\Delta U_i^{\ell-1} + 9U_i^{\ell-2} - 2U_i^{\ell-3}}{6} \tag{3.26}$$

Where n correspond to the value within current pseudo loop and values with superscript $\ell - i$ are those stored from previous real time steps.

In case flow is turbulent, in the same manner a transient term need to be added in the transport equation 3.15 to recover solution, the approximation used are same backward difference formulae described above, could be written for $\hat{\nu}$.

3.6 Initial and Boundary conditions for modelling blood:

The governing equations in the discretized form have been presented. However, in order to close the system of equations so that solution procedure can be initiated additional information is required, usually provided with, in term of initial and boundary conditions.

3.6.1 Initial conditions:

Solution of fluid problems involving transient terms, demands to prescribe the value of field variables at some reference time, to start with computation. The flow field has been modelled by introducing artificial compressibility, in which case it does not matter that required solution is steady or transient, in either case initial conditions are defined. However, for steady state solution free stream values can serve this purpose; however for transient problems special considerations should be given while initializing the variables, so that resulting initial conditions are reasonable and physically correct. In this work for steady state solution initial conditions used are free stream values with zero values. Whereas, for recovering transient solution first steady state simulations carried out to initialize the field variables.

3.6.2 Boundary conditions:

The boundary conditions are defined on the wall of artery and cross sections. For blood modelling on the wall of arteries non-slip conditions with both of normal and tangential component of velocity equal to zero are prescribed. On the inlet and outlet cross sections of a blood conduit transient velocity profile is defined. To date there are two most commonly employed profiles used to prescribe velocity field, including those either given by Womersley, or obtained as a solution of Helmholtz equation. However, in the current study velocity profile applied are those obtained as a numerical solution of helmholtz equation.

3.6.3 Numerical solution of Helomholtz equation:

Numerical solution technique can be employed to obtain a transient velocity profile, which is in contrast to Womersley profile is not limited to any specific cross section. It involves the finite element solution of the Naiver stoke equations. The incompressible Navier stoke equation in vector form can be written as:

$$\begin{gathered} \frac{\partial \vec{u}}{\partial t} + (\vec{u} \cdot \nabla)\vec{u} - \nu \nabla^2 \vec{u} = \frac{\nabla p}{\rho} \\ \nabla . \vec{u} = 0 \end{gathered} \tag{3.27}$$

Applying Naiver stoke equation, to the pipe flow problem, and using Fourier transform, for nth harmonic the system of equations can be reduced to a following boundary value

problem:

$$\nabla_{\perp}^{2}\tilde{u}_n + \kappa_n^2\tilde{u}_n = f_n; \quad \text{where } \nabla_{\perp} = [\partial_x, \partial_y]^T \\ \tilde{u}_n = 0 \in [\Omega] \tag{3.28}$$

Where $\kappa_n = \sqrt{-iw_n/\nu}$ is called stoke viscous wave number and $f_n = (\tilde{p}_z)_n/\nu\rho$. The above equation 3.28, is a non-homogeneous two dimensional partial differential equation often called as Helmholtz equation in mathematical context, which reduces to the poisson equation as a special case for $n = 0$. The procedure adopted to computed time varying velocity profile is same as described in the [99], and is briefly mentioned here:

Since ultrasonic measurements provide with transient velocity profile at the centre line of blood vessel, the velocity profile employed in the current study is obtained from the clinical data. The Fourier fast transform is used to calculate complex amplitude $\tilde{U}_n$. Then for a particular cross section the surface mesh is first transformed into a horizontal $2\mathbb{D}$ plane mesh, by rotating along the geometric centre, which is used for the numerical solution by employing finite element discretization of Helmholtz equation. From the solution obtained, the centreline is found by locating a point (x_c, y_c) which correspond to the maximum value of the computed velocity. The numerical solution obtained for N harmonics is then normalized $(\tilde{\nu}_n)$ by dividing with centreline value of velocity. Now velocity profile can be computed at section by the following expression:

$$u(x, y, t) = \sum_{n=-N}^{N} \tilde{U}_n\tilde{\nu}_n(x, y)e^{i\omega_n t}$$

The same procedure can also used for computing velocity profile at the outlet, where flow rate are usually, defined as percentage of inlet flow rate.

3.6.4 Initial and boundary condition for transport equation:

For the turbulent flow Sparlart Allmaras model has been used, the solution of which requires to prescribe initial and boundary conditions. The initial and inflow boundary condition are usually set in term of $\tilde{\nu}$, with a value less than $0.1 \times \nu$, where ν is the kinematic viscosity and $\tilde{\nu}$ is the turbulence kinematic eddy viscosity. However, on the solid wall no-slip boundary condition is assigned, whereas at outlet it is not necessary to prescribe any condition as these value are extrapolated from values in the domain [9, 14].

Chapter 4

Performance of codes, and analysis of aneurysm inflicted model artery

For the solution of incompressible Naiver stoke equations, in-house computational codes implemented in the Fortran have been used, on the in-house computing system. Before proceeding toward blood flow simulation in the aorta, first in order to validate and check the performance of the codes, a test case has been considered.

4.1 Performance of codes, and cavity flow problem:

In computational fluid dynamic, cavity flow problem is regarded as the benchmark, which is commonly employed to check performance of computational codes and numerical schemes. A square cavity with unitary sides, where $2\mathbb{D}$ steady incompressible flow field driven by horizontal movement of top wall, is modelled for the purpose of evaluation. Cavity flow problem, in addition to the simplicity of its geometry, provide with complex fluid flow physics, due to development of recirculating regions near the corners edges. Non uniform unstructured mesh has been used, where no-slip boundary conditions are prescribed on the three solid walls, with top lid moving along x-direction with unit velocity. The algorithm used in this work, when applied to the cavity flow problem in semi-implicit form, can give steady state solution up to Reynold as high as 5000. In order to compare the results, it is common practice to plot horizontal velocity (u) and vertical velocity (v) along the vertical and horizontal lines passing through geometric centre of the domain, respectively. The results for the velocity components, obtained have been shown in the figures 4.1 and 4.2. It can be noticed that for higher Reynold number influence zone of recirculation is more predominant and more frequent.

Numerous studies have been carried out to investigate characteristics of the flow in the lid-driven cavity. An analysis of the reported data shows that up to Reynold number 1000, there are almost same results by different researchers. However for higher Reynold number, some researchers have found that it behaves as non-steady, $3\mathbb{D}$ and periodic flow, while other

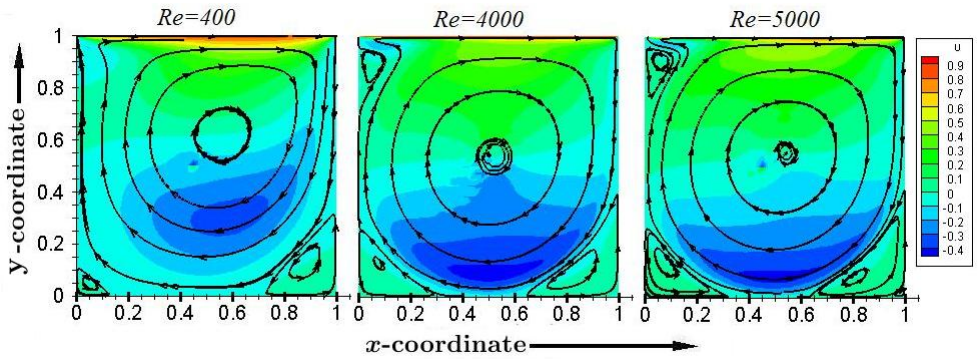

Figure 4.1: Velocity contour plot at different Reynold number

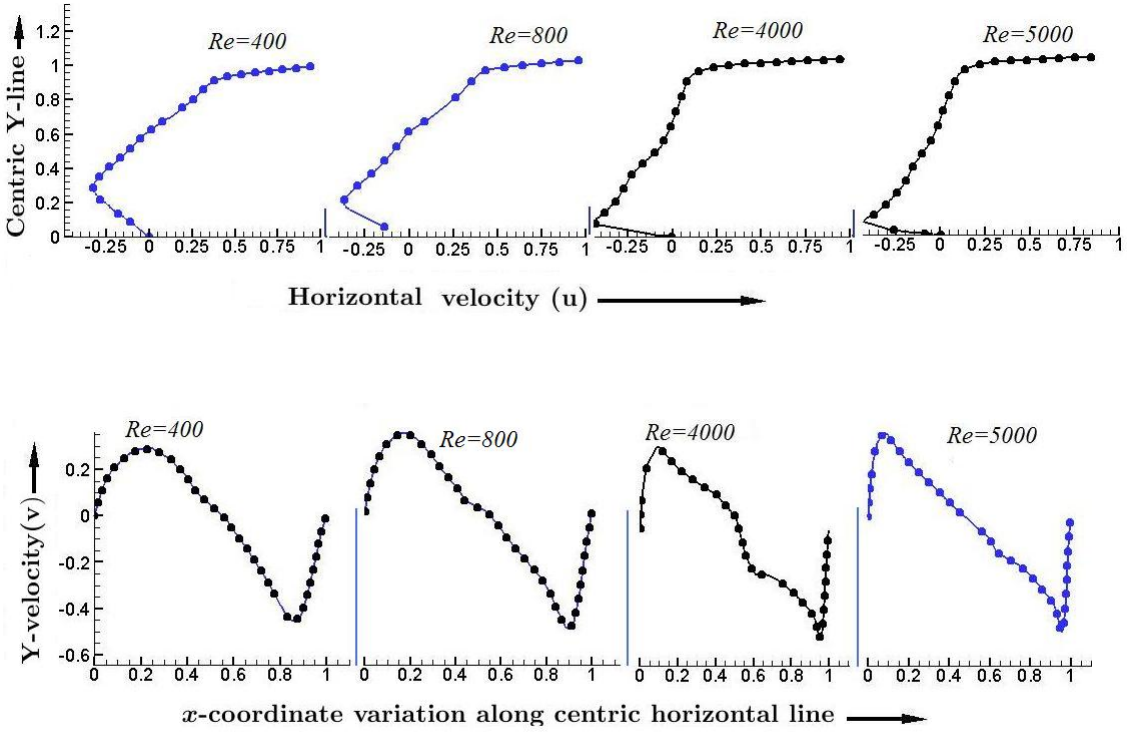

Figure 4.2: Velocities variation along the horizontal, and vertical line passing through centre

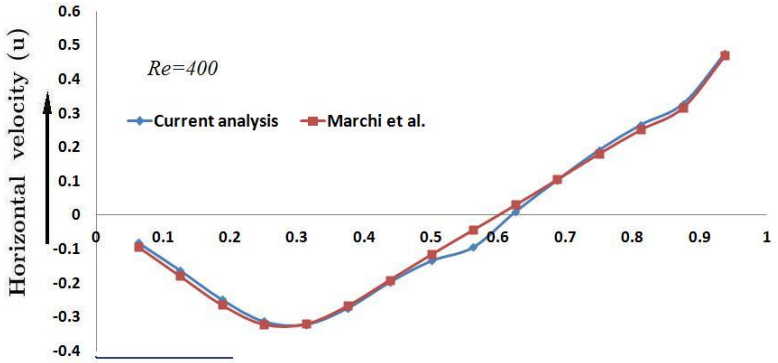

(a) Comparison at Re=400

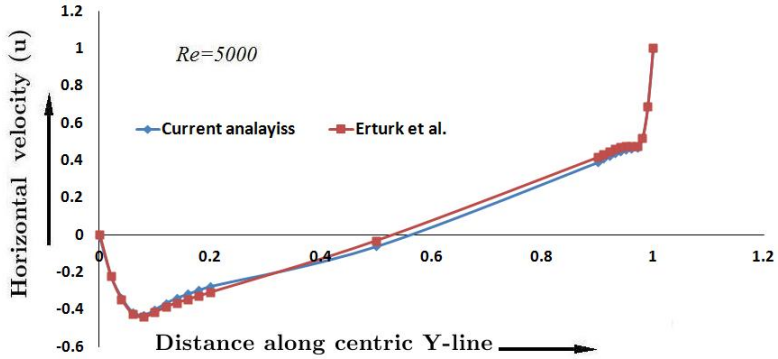

(b) Comparison at Re=5000

Figure 4.3: Comparison with the results reported by Marchi et al. [69] for Re=400, and with those of Erturk et al.[31] at Re=5000

have obtained solution [31, 32, 90], thus it can be argued that nature of flow is not agreed upon for higher Reynold number. Marchi et al. [69], have carried out analysis of the cavity problem with refined grid 1024×1024 and by employing finite volume discretization. They have presented the most accurate solution, for Reynold number ≤ 1000, thus is considered as reference. Erturk et al.[31] have also studied same model problem but at high Reynold number, and obtained steady state solution for Reynold number up to 21000, hence taken as reference for analysing flow at high Reynold number. In order to validate the codes, two cases with $Re = 400$ and $Re = 5000$, have been compared as shown in the figure 4.3, where results are in complete agreement with reference values, and thus can be used for blood modelling without any apprehensions associated with the codes performance.

4.2 Model blood vessel:

This section has been designed as a preliminary study to analyse unsteady, fully developed pulsatile flow, in a model vessel. The model artery considered resembles to the carotid

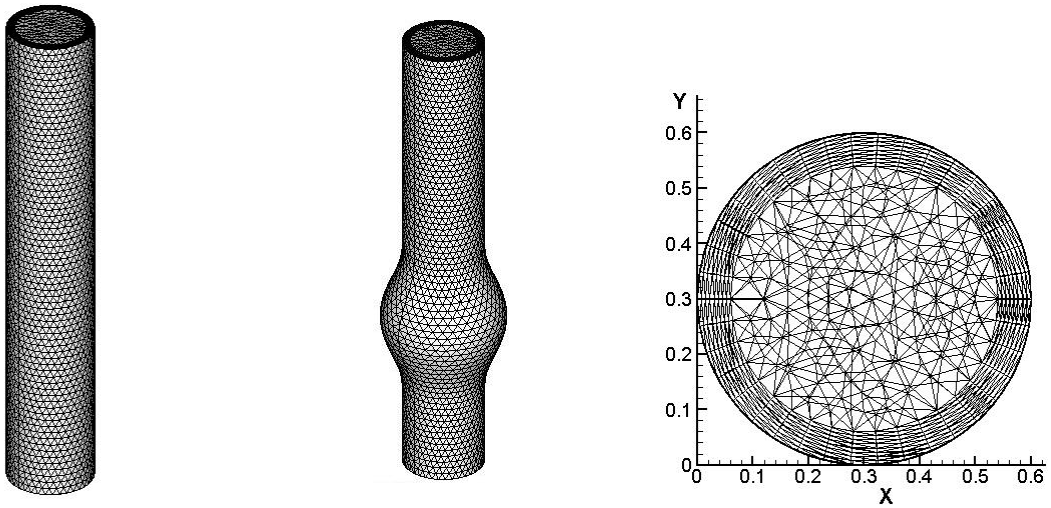

(a) Normal model aorta

(b) Aneurysmal aorta with dilation by 50 %

(c) Cross sectional view, representing boundary annuli

Figure 4.4: Healthy and diseased Model artery, with meshed geometries

artery in dimensions and flow rates, which is less likely to be effected by aneurysm in reality. However, the sole motive behind this study is to perform comparative analysis in the healthy and diseased model vessel, in order to check aneurysm induced flow variations, by observing hemodynamics and flow parameters. A model blood vessel having diameter $0.6cm$ is considered as a reference, where a fusiform aneurysm representing focal dilatation has been modelled. Two different cases will be studied, one with normal healthy artery, with which results of other case having aneurysm bulge enlarged by 50% with respect to the normal size, would be compared, as shown in the figure 4.4.

4.2.1 Grid Generation and mathematical model

For grid generation purpose, in-house computational codes ($FLITE3D$) has been employed. Figures 4.4a and 4.4b, represent the model blood vessels meshed with tetrahedra elements, where mesh density is concentrated in the in outer annuli with 8 boundary layers, as shown in the figure 4.4c. The domain of problem is meshed with 169666 elements connected through 30088 nodes. The desired problem, has been modelled by Naiver stoke equations, under the assumptions that blood flow is incompressible, laminar, unsteady, and Newtonian, which are valid approximations for large blood vessels. The techniques used based on CBS-AC algorithm for discretization, where dual time stepping scheme is employed to recover transient solution.

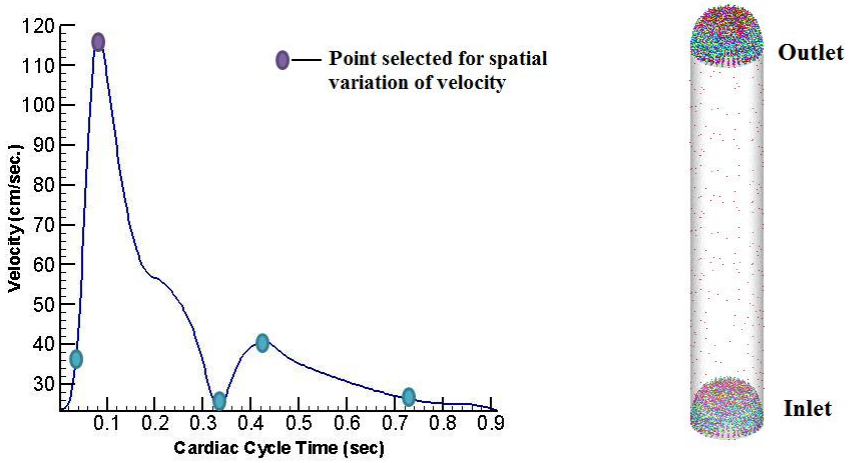

(a) Transient velocity profile

(b) Velocity profile at the inlet and outlet sections

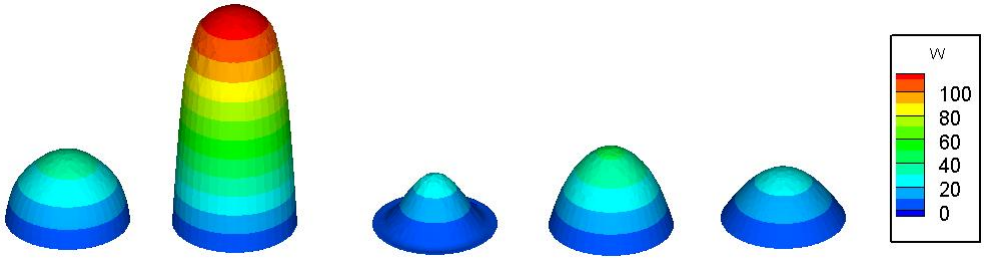

(c) Spatial variation of velocity profile at selected point from left to right respectively

Figure 4.5: Spatial and temporal variation of applied velocity profiles

4.2.2 Boundary condition and solution procedure

The boundary condition prescribed on the solid wall are those of non-slip type. However, to model periodic pulsatile flow, transient velocity profiles are defined at both inlet and outlet. For this analysis time period assumed is ≈ 0.92 *sec*, and velocity profile applied are those obtained as a numerical solution of Helmoholtz equation, by assuming flow rate equal to 6 cm^3/sec. The peak velocity is 116 cm/s that appears at time instant of $0.085s$, during a cardiac cycle. The resulting velocity profile with its both spatial and temporal variations, has been shown in the figure 4.5. The solution algorithm used is based on the non-dimensional form of governing equations. The initial conditions described are in term of free stream values of pressure and velocity, having zero magnitude. The resulting flow field has been solved for one complete cardiac cycle, by dividing total physical time into 240 parts, which results into a small time step, found to ensure convergence.

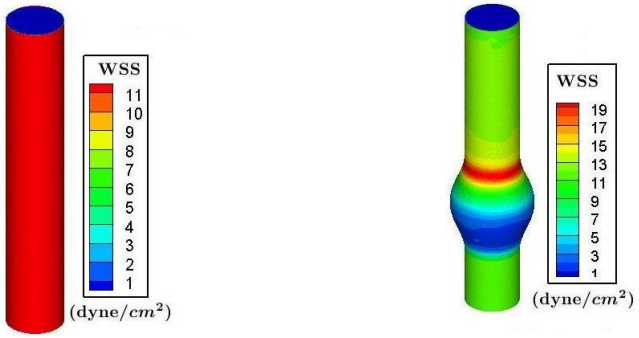

(a) WSS plot, for the straight model artery

(b) WSS variation in case there is aneurysm

Figure 4.6: Contour plot of wall shear stress with reduced flow rate

4.2.3 Results and discussion:

The vascular diseases involving stenosis and aneurysm, results into disturbed blood flow with circulation and stagnant flow zones. The hemodynamic parameters usually studied to define wall mechanic of a diseased artery are those including wall shear stress and oscillatory shear index (OSI) [52] as described in section 2.2. This study is carried out by exploiting the variations of the wall shear stress (WSS) and oscillatory shear index (OSI), where an attempt has been made to establish an association between local hemodynamic parameters and aneurysm effected areas. The non-dimensional scale employed are similar to those mentioned earlier, with resulting Reynold number equal to 1833.

WSS variations:

Figure 4.6 represent time averaged variations of wall shear along the length, in both healthy and diseased model arteries. It can be noticed that in case of straight model artery, the wall shear stress remains nearly, constant along the length. However, in case there is a fictitious aneurysm wall shear stress has completely different pattern. The maximum mean wall shear stress observed is 19 dyne/cm^2, and minimum value is approximately, 1 dyne/cm^2 located at aneurysm site. The high level of wall shear stress at proximal and distal sites of aneurysm explained as a result of curvature and centrifugal effects induced by geometry changes. The temporal variation of instantaneous peak wall shear stress is represented in the figure 4.8. The instantaneous wall shear stress is significantly higher than the mean value, stands as high as 190 dyne/cm^2, found in this study. Since wall shear stress is defined as the gradient of the velocity field, therefore in a simple model geometry the temporal variation follows same trend as that of velocity.

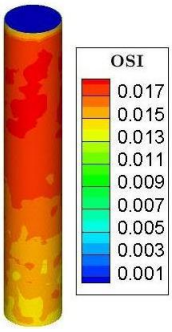

(a) OSI contour plot for healthy model artery

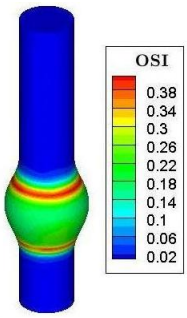

(b) OSI variations, in the aneurysm inflicted model artery

Figure 4.7: Comparative contour plot of oscillatory shear index (OSI) variation

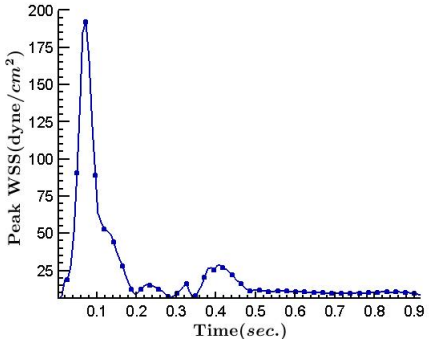

Figure 4.8: Plot of instantaneous Peak wall shear stress, over cardiac cycle

Contour plot of OSI

The dramatic changes in the transient WSS stress can be described via contour plot of oscillatory shear index (OSI), as shown in the figure 4.7. The higher value of OSI at a point, can be interpreted as the site with increased residence time of fluid particles. In case there is no aneurysm, the flow is smooth without having any retrogradations, and hence value of oscillatory shear index will be negligible, as can be seen from figure 4.7a. On the other hand OSI is high for the locations where there is bulge or aneurysm. The maximum value of OSI is 0.5, however in this study it reaches to 0.38 as shown in the figure 4.7b, representing the increased risk of reverse flow.

An additional case with reduced flow rate:

Before proceeding to conclude any remark from the above analysis, an other case is considered where flow rate is reduced up to half of the original value i.e. Reynold number is decreased. The modification will change corresponding velocity profile, thereby resulting

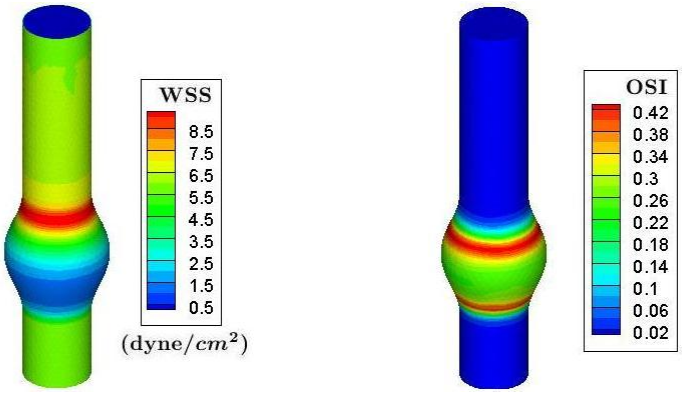

(a) WSS variation in case there is aneurysm

(b) OSI variation, for model artery inflicted with aneurysm

Figure 4.9: Contour plot representing variations of Wall shear stress (WSS) and Oscillatory shear index, in case of reduced flow rate

into dropped wall shear stress since it depends upon the Reynold number [143]. In order to conform with the obvious observations, the result has been plotted in the figure 4.9, where it can be visualized that wall shear stress has lowered to nearly half of the value found in the original case. Moreover, the variations of WSS along the length of the model follow, the same pattern with respect to maximal and minimal values. Contour plot for OSI, has also been shown having exactly, similar trend to that of the previously studied case.

4.2.4 Summary:

The result of model analysis are summarized as

- The site of aneurysm is directly associated with the low level of wall shear stress.
- OSI indicates that the aneurysm inflicted portion of blood vessel is relatively, at increased risk of stagnant flow.

On the basis of this data it can be concluded that at a location the combination of lower WSS and higher OSI dictate the pathogenesis of aneurysm. Thus these parameters are quite useful, in studying the flow pattern in the diseased blood vessels, where one can predict consequence for patient suffering from aneurysm. Currently, it has also been advocated that risk of aneurysm rupture and decision regarding aneurysm treatment, should also be based on the CFD analysis involving calculation of wall shear stress.

Chapter 5

Modelling of patient specific aneurysm

5.1 Significance of hymodynamic parameter in chracterising risk factors associated with aneurysm:

The vascular diseases involving stenosis and aneurysm, usually result into disturbed blood flow with circulation and stagnant flow zones, thereby providing with ample time for the accumulation of leukocytes and hence atherosclerosis [103]. It has now been well established fact that level of wall shear stress can characterise the risk associated with the development, progression and rupture of aneurysm [103, 55, 111, 106, 83]. Since shear stress quantifies the mechanical forces acting upon the blood vessel, therefore can control intra-vascular process, which causes proliferation of neo-intimate layer, hence leads toward vessel remodelling [103]. Silber et al. [106] have studied the response of endothelial dysfunction in vasodilation with respect to wall shear stress and found that they are closely interrelated with each other. Low wall shear stress is often found, in the regions where flow is unstable. In several experimental and clinical studies [55, 15, 134] it has been documented that vascular regions with low wall shear stress are at the increased risk of atherosclerosis formation. The wall shear stress because of pulsatile nature of flow has, maximum value at the peak systole [111].

Papaioannou et al. [83] have reviewed the available data for wall shear stress in the blood vessels and reported that among the different studies it varies between $10 - 70$ dyne/cm^2, with a mean shear stress level lies in the range $11 - 15 dyne/cm^2$. Similar results were demonstrated by Reneman et. al. [92]. In the hostile anatomy of a blood vessel, which include high curvature and branching points, higher values have been found in the literature [15]. It has been found that regions with wall shear stress $\leq$ 4dyne/cm^2 are not protected against the atherosclerosis deposition [143, 52]. Despite of these studies, it is difficult to set exact limiting values of the wall shear stress at a particular site, because it is highly dependent on the flow parameters and boundary layer mesh employed to carry out CFD

study.

5.2 Aneurysm inflicted patient specific case:

Aorta is the largest blood vessel, often found to be effected by the aneurysm, a detailed description of aortic aneurysm has been given in the chapter 1. In this unit a patient specific case, having aneurysm is studied, to examine the localisation of hymodynamic parameters and their association with arterial dysfunction, as a result of disturbed flow. The patient specific case considered, has an aneurysm at the downstream, near the folded neck as shown in the figure 5.1a, usually called as thoraco-abdominal aortic aneurysm. The bulge is of fusiform with the size approximately equal to $5cm$. In addition to aortic arch which introduces centrifugal effects, there is unexpected distortion of the geometry of aorta, which would further complicate the current study. The patient specific model has been analysed at peak Reynold number of 2500, which is usually studied, for blood modelling through thoracic aorta [104].

5.3 Defining problem for analysis and preprocessing:

5.3.1 Constructing surface and volume mesh from CT-scans:

Computed tomography (CT) scan were obtained from the Morisston hospital of a thoracic aortic aneurysm patient. Mesh is constructed by extracting information from CT-scans. First, the surface mesh is generated by region segmentation of scans by employing commercial software AMIRA, from which stereolithiographic(STL) file is obtained. Then volume mesh is constructed by employing in-house computational codes. The generation of mesh involves number of cosmetic operations, including edge contraction and edge swapping and local taubing smoothing as described in [8, 99]. Since the main focus is to model blood flow in the aneurysm inflicted area, thus final geometry can be simplified by clipping the abdominal portion and side branches, however small extension were kept for brachiocephalic trunk, left common carotid artery and left subclavian artery as shown in the figure 5.1b. This is followed by the structured boundary layer mesh, then transformed into volume mesh by Delaunay triangulation. There is annuli of 10 structured boundary layer, with mean element edge length equal to $0.04mm$. The domain of the problem in hand is discretized with tetrahedra elements, which accounts to 3311878 connected through 570923 number of nodes, the final mesh thus obtained is shown in the figure 5.1.

5.3.2 Numerical model and boundary conditions:

The numerically model is defined by the set of Naiver stoke equations as described in the section 2.3. The blood flow simulation, is carried out while assuming that flow field is incompressible, unsteady and Newtonian. However, as according to reported results that flow in the diseased aorta, specially, in the ascending aorta and aortic arch, flow is prone to

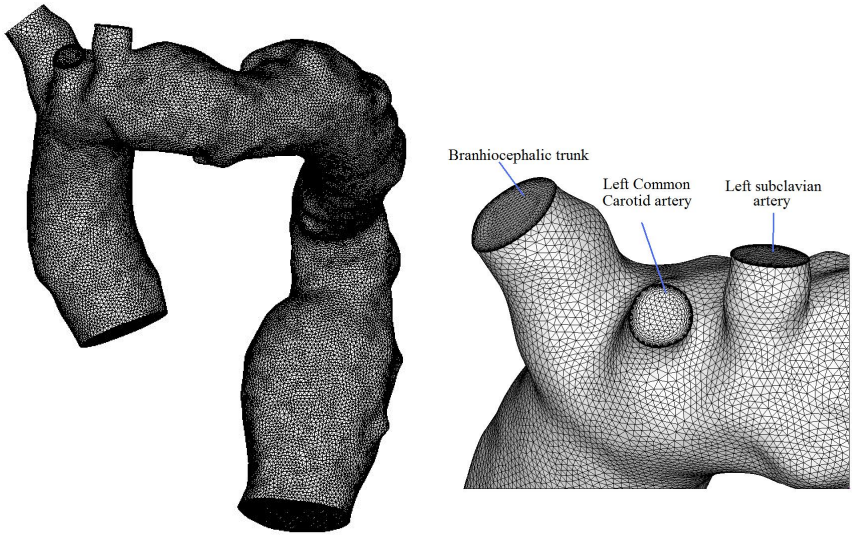

(a) Mesh of patient specific thoracic aorta

(b) A close view of branch artereris and boundary layer mesh

Figure 5.1: Mesh with tetrahedra elements employed for domain disrectization of aorta

turbulence therefore, modelled as turbulent in this study. For modelling turbulence Sparlart Allmaras model has been employed, discussed in section 2.4.1. Thus 3$\mathbb{D}$ Naiver stoke equations in concert with turbulence model are solved for the solution of problem.

The algorithm used is CBS-AC scheme with dual time stepping scheme to retrieve transient solution. The system of equations is completed by defining non-slip boundary condition on the solid wall and prescribing transient velocity profile at the inlet and outlet. Since there is one inlet and four outlet, therefore flow division is required. Flow division is assumed as 66%, 17 %, 10% and 7% for downstream outlet, Brachiocephalic trunk, left common carotid artery and left subclavian artery respectively. The time period used for cardiac cycle is taken to be equal to 0.61 *sec.*. In order to initialize the variables for carrying out unsteady simulation, first a steady state solution at same flow conditions is obtained. The time period of cardiac cycle is divided into 240 equal parts, resulting into a small time step, found to ensure solution convergence. The criterion for convergence, is given in term of L2 norm of velocity by predefining its value equal to 10^{-5}.

5.4 Results and local hemodynamics parameters:

To investigate the flow structure, hymodynamical parameter considered are those including wall shear stress, pressure and oscillatory shear index variations. Pressure and wall shear stress are regarded as the most relevant parameters, for blood flow involvement in the devel-

opment of atheroma [104]. The variations of pressure are illustrated in the figure 5.2, three different time instant corresponding to peak systolic acceleration, systolic deceleration and late diastole respectively are considered as shown in the figure 5.2a. It can be seen that during the early systole pressure in high in the ascending aorta, which is equal to 26656 dyne/cm^2, the highest cyclic value. Then as time progress pressure concentrated region is visualized, not only transferring toward the arch and further descending aorta but also diminishes in magnitude. The value of peak pressure at the late diastole dropped by almost up to 35% of the pressure observed at the peak systole.

Since problem is transient, WSS is studied as time averaged variable. The maximum wall shear stress found is equal to 53.26 dyne/ cm^2, located at the proximal site to the aneurysm as shown in the figure 5.3b. It can be observed that wall shear stress is significantly higher at the base of branch arteries as represented in the figure 5.3c. However, at the location of aneurysm the values of wall shear stress is lowest.

In order to assess the temporal variation of peak wall shear stress three time instants were selected similar to those used for analysing pressure variations. From the figure 5.2c, it can be suggested that at the peak systole wall shear stress is highest at the inlet, which is result of impingement of fluid particle at entrance. Then during the deceleration phase, a reduction in the level of peak wall shear stress was observed. However, at the late diastole high value of peak wall shear noticed at the proximal site of aneurysm due to change in the geometry, as particles has to turn by almost 90° to enter into aneurysm portion, thereby increase shear rate and hence shear stress.

Figure 5.4, represent plot of oscillatory shear index. As thoracic aorta involves aortic arch, which can develop secondary flow and hence high oscillatory shear index because of evident centrifugal effects. The maximum value of OSI is equal 0.495, found at the site of aneurysm. The region of lower wall shear stress are more prone to the reversal flow, which is responsible for further atherosclerosis and aneurysm enlargement. Thus, it supports the argument that aneurysm continue to grow in size until rupture at one or more sites occurs.

The regions where wall shear stress is high, can be explained by the presence of aortic arch and centrifugal effects, since as fluid particle move in a curved arch they impinge with wall thereby increase shear rate and hence shear stress. The most effected region with WSS is the proximal site of the aneurysm, where fluid particle changes direction by almost 90°, thereby inducing high frictional force on the sharp bend and hence shear stress is also increased. Shahcheraghi et. al.[104] carried out a model study for blood flow in aortic arch and reported that curvature of aortic arch and presence of branch arteries introduces secondary flow. Thus, result of this study representing high values of OSI along the length of aorta are in agreement with their observation. Wall shear stress remains low throughout cardiac cycle at the site of aneurysm, however at other location it varies with Peak systole and diastole. At the branch point wall shear stress is also higher, which is a result of flow

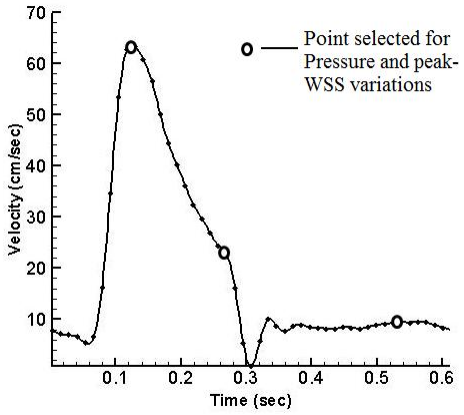

(a) Selected point shown on velocity profile

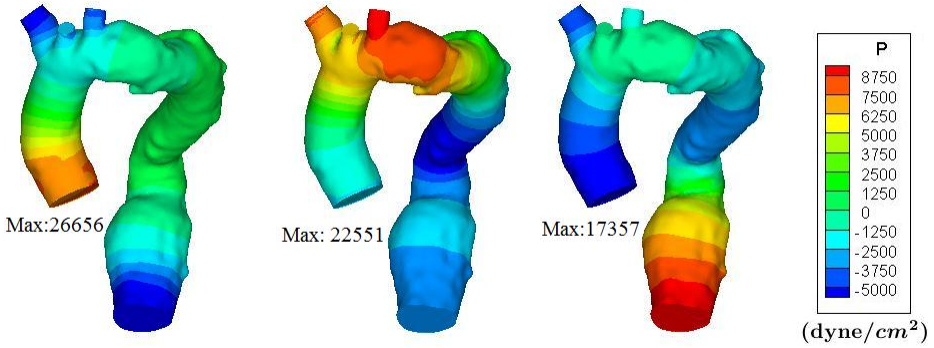

(b) Instantaneous pressure variation at different time instant over cardiac cycle

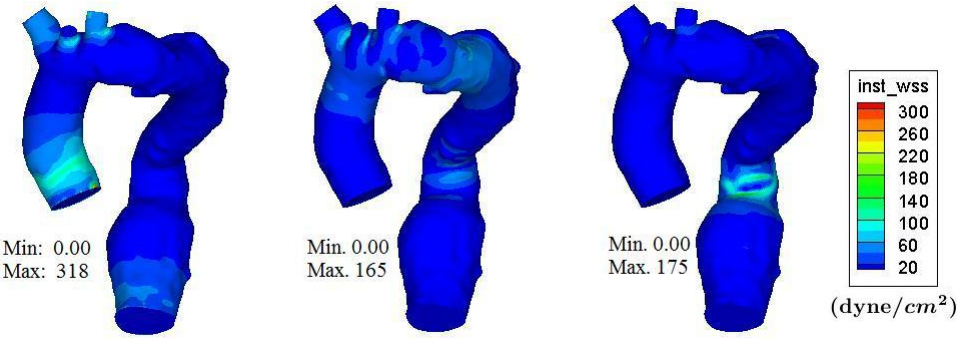

(c) Instantaneous wall shear stress variation at different time levels over cardiac cycle

Figure 5.2: Contour plot of representing pressure and wall shear stress variation as time progress

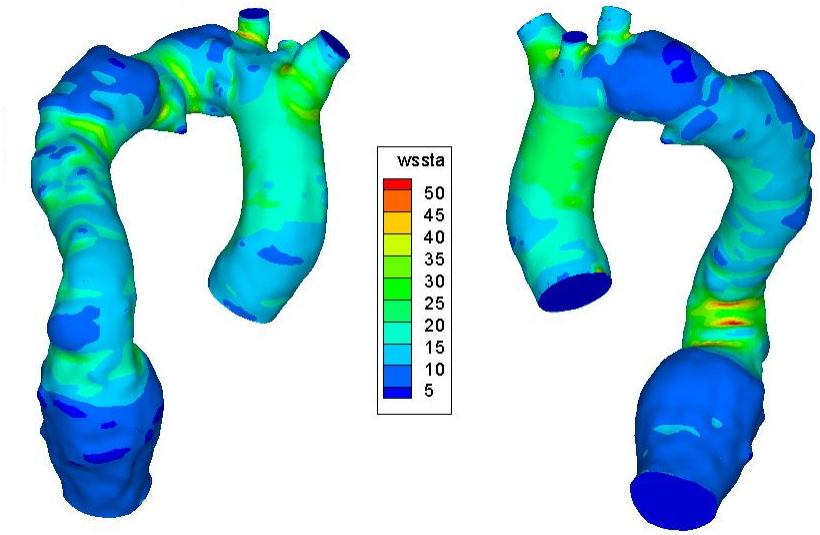

(a) Contour plot of WSS

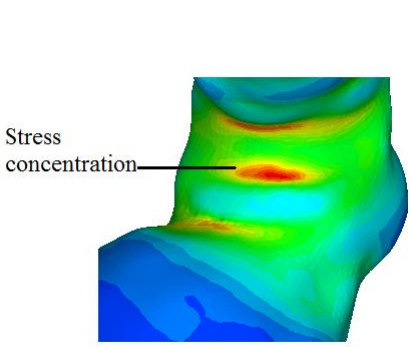

(b) Region of Stress concentration

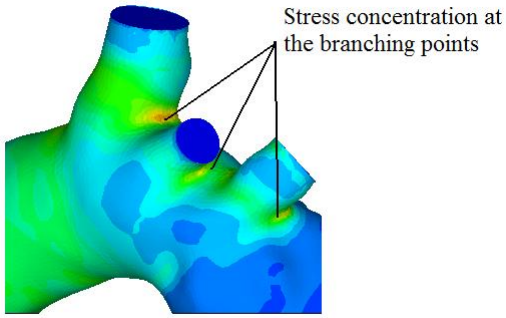

(c) Stress concentration at the branches locations

Figure 5.3: Contour plot of time averaged WSS for patient specific case, along with regions of stress concentrations

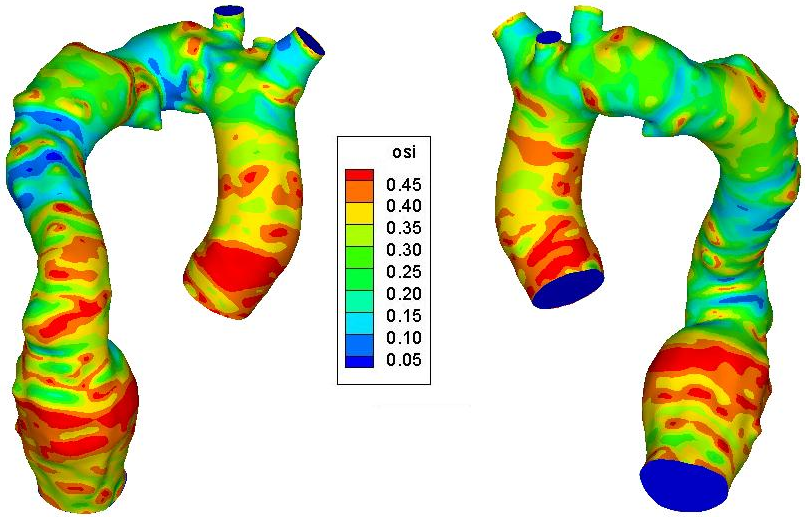

Figure 5.4: Contour plot of Oscillatory shear index (OSI)

separation, causes disturbance at that location.

5.5 Additional case with symmetric geometry

In order to verify the above stated observations, an additional case is considered. The trend of these results is of interest as these are obtained at very low flow rates. This additional problem is solved by implementing same procedure as discussed in the solution of the previous case. The variation of wall shear stress and oscillatory shear index are shown in the figure 5.5. The maximum wall shear stress is located at the aortic arch, and in the branch vessels. Because of constriction offered by the small branch vessel, there is high frictional force, which in turn results into higher shear stresses level. From the geometry it can be visualized that, complete ascending aorta is effected by the aneurysm, therefore it can be seen that oscillatory shear index is significantly higher in that diseased region. Since the geometry is symmetric, thus results are very much predictable, i.e. at the site of aneurysm WSS is lowest and OSI has highest value, compared with those of other domain, this fact already documented in the section 4.2, and further illustrated here.

5.6 Summary:

Results presented can be summarized as pressure and wall shear stress varies along the cardiac cycle with peak values at the peak systole. The maximum value of wall shear was found to be equal to 53dyne/cm^2, which lies in the range reported by the [83]. The wall shear stress was observed to be concentrated at the site where there is either branch point, bend or kink is present. Due the high centrifugal effect and flow division at the branch arteries

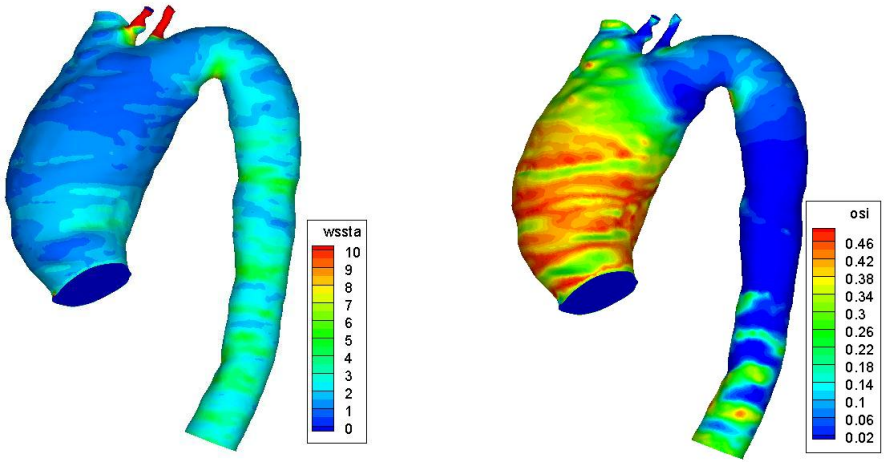

(a) Wall shear stress (b) OSI contour plot

Figure 5.5: WSS and OSI for an additional case, with reduced flow rate

flow remains disturbed and secondary flow become evident along the length of aorta. At the site of aneurysm wall shear stress is lower and oscillatory shear index is highest, therefore an existing aneurysm is more prone to atherosclerosis. Therefore, aneurysm should be repaired otherwise it will continue to grow in size. Thus this study advocates the use of CFD tool, can characterise the risk factor associated with the aneurysm.

5.7 Conclusions and Future directions:

This work largely can be divided into three sections, where first is devoted to the investigation of current status of aortic aneurysm. Since aneurysm is irreversible focal dilatation of an artery, which continues to grow in size until it ruptures. The issue that when, one should intervene to treat the aneurysm is still unresolved. Although some studies report that once a limiting size is reached then it should be repaired, but this argument is contradicted by those cases for which aneurysm ruptures even before crossing the threshold limit. However, currently it has been reported that use of CFD tool for the watchful surveillance could provide with an alternative technique. In second section the mathematical model was developed by, employing $3\mathbb{D}$ Naiver stoke equations in conjunction with artificial compressibility. Where, temporal and spatial discretizations are carried out by characteristic Galerkin and standard Galerkin procedure respectively. For modelling turbulence in the diseased blood vessel Sparlart-Allmaras turbulence model was employed. Then after verification of code by a test case, this is followed by the blood flow modelling of, model and patient specific cases.

A comparative study involving healthy and diseased model artery with fictitious aneurysm is investigated. This shows that for artery inflicted with aneurysm, the wall shear stress is low and oscillatory shear index is higher at the site of bulge, which is found in agreement with other findings. Then blood flow simulation of a patient specific aneurysm is carried out. The analysis suggested that at a peak systole when pressure is significantly higher, the wall shear stress was also found to have markedly high value. The time averaged wall shear stress was found to equal to values reported in the literature. The analysis carried out can be summarized as the region with high wall shear and low oscillatory shear index, is usually a diseased area, and is at the higher risk of atheroscelrosis. This study also support the argument that aneurysm continues to grow in size, this is because diseased region is more prone to atherogenesis and hence enlargement. A supplementary case was also studied, with the same localisation trend of WSS and OSI, and thus verifying these observations.

Although realistic study has been performed, by constructing mesh from CT-scans, the truncation of the aorta and removing side branches results into approximation of actual geometry. The transient solution sought by prescribing transient velocity profiles, which were developed and applied by assuming inlet and outlet as a plane section. However, in reality they are not plane sections. In order to extend this work, wall mechanic of blood vessel should also be investigated, which requires fluid structure analysis (FSI), to be carried out. Finally, to implement idea of calculating hemodynamical parameters in the field, requires to develop some kind of CFD based software tool, thereby minimizing gap between the people in the field and those in the engineering community.

Appendix A

Matrix Algebra

A.1 Turbulence parameters for Sparlart-Allmaras model

Where parameters used are defined as:

$$\widetilde{\Omega} = \Omega + f_{\nu 2}\left(\frac{\widetilde{\nu}}{(\kappa y)^2}\right)$$

Ω is mean vorticity computed by

$$\Omega = \sqrt{\left(\frac{\partial u_i}{\partial x_j} - \frac{\partial u_j}{\partial x_i}\right)^2}$$

$f_{\nu 2}$ and f_w are other kinds of wall damping functions, y is distance from nearest wall

$$f_{\nu 2} = 1 - \frac{\chi}{1 + \chi f_{\nu 1}}$$

$$f_w = g\left(\frac{1 + C_{w3}^6}{g^6 + C_{w3}^6}\right), \quad g = r + C_{w2}(r^6 - r), \quad r = \frac{\widetilde{\nu}}{\widetilde{\Omega}(\kappa y)^2}$$

whereas, constants C_{wi} are given as

$$C_{w1} = C_{b1} + \kappa^2 \frac{1 + C_{b2}}{\sigma_{\widetilde{\nu}}}, \quad C_{w2} = 0.3, \quad C_{w3} = 2$$

The values used for other remaining constants are $\sigma_{\widetilde{\nu}} = 2/3,\ \kappa = 0.4187,\ C_{b1} = 0.1355,\ C_{b2} = 0.622$ [8, 126].

A.2 Matrices used for spatial discretization

$$\begin{gathered}\mathbf{M}_u = \int_\Omega \mathbf{N}_u^T \mathbf{N}_u d\Omega; \quad \mathbf{C_u} = \int_\Omega \mathbf{N}_u^T \left(\frac{\partial}{\partial \mathbf{x}_j}(\widetilde{\mathbf{u}}_j \mathbf{N}_u)\right) d\Omega; \quad \mathbf{K}_\tau = \frac{1}{Re}\int_\Omega \frac{\partial \mathbf{N}_u^T}{\partial \mathbf{x}_j}\tau_{ij} d\Omega \\ \mathbf{f} = \frac{1}{Re}\int_\Omega \mathbf{N}_u^T \mathbf{t}^d d\Omega; \qquad \mathbf{K}_u = -\frac{1}{2}\int_\Omega \frac{\partial}{\partial \mathbf{x}_k}(\mathbf{N}_u^T \mathbf{u}_k)\frac{\partial}{\partial \mathbf{x}_j}(\mathbf{N}_u \widetilde{\mathbf{u}}_j) d\Omega\end{gathered} \tag{A.1}$$

pressure equation

$$\mathbf{M}_p = \int_\Omega \mathbf{N}_p^T \mathbf{N}_p d\Omega; \quad \mathbf{H} = \int_\Omega (\nabla \mathbf{N}_p)^T (\nabla \mathbf{N}_p) d\Omega; \quad \mathbf{G} = \int_\Omega (\nabla \mathbf{N}_p)^T \mathbf{N}_u d\Omega$$
$$\mathbf{f}_p = \int_\Gamma \mathbf{N}_p^T \mathbf{n}^T \left[\tilde{\mathbf{U}}^n + \theta_1 \left(\Delta \tilde{\mathbf{U}}^{\mathbf{inter}} - \Delta t \nabla \mathbf{p}^{n+\theta_2} \right) \right] d\Gamma \tag{A.2}$$

Where matrices $\mathbf{M}_u$ and $\mathbf{G}^T$ are already defined; however, matrix $\mathbf{L}$ is given as:

$$\mathbf{L} = \frac{1}{2} \int_\Omega (\nabla(\mathbf{u}\mathbf{N}_\mathbf{u}))^T \nabla \mathbf{N}_p d\Omega$$

A.3 Spatial discretization of transport equation

$$\mathbf{M}_\nu = \int_\Omega \mathbf{N}^T \mathbf{N} d\Omega; \quad \mathbf{C}_{\nu_1} = \int_\Omega \frac{\partial \mathbf{N}^T}{\partial \mathbf{x}_i} \mathbf{N} \{\hat{\nu} \mathbf{u_i}\} d\Omega;$$
$$\mathbf{K}_{\nu_1} = -\frac{1}{Re\sigma_{\tilde{\nu}}} \int_\Omega \frac{\partial \mathbf{N}^T}{\partial \mathbf{x}_i} (1+\hat{\nu}) \frac{\partial \mathbf{N}}{\partial x_i} \{\hat{\nu}\} d\Omega + \frac{C_{b_2}}{Re\sigma_{\tilde{\nu}}} \int_\Omega \mathbf{N}^T \left(\frac{\partial \mathbf{N}}{\partial \mathbf{x}_i} \{\hat{\nu}\} \right)^2 d\Omega$$
$$+C_{b_1} \int_\Omega \mathbf{N}^T \mathbf{N} \hat{\Omega} \{\hat{\nu}\} d\Omega - \frac{C_{w_1} f_w}{Re} \int_\Omega \mathbf{N}^T \mathbf{N} \left\{ \left(\frac{\hat{\nu}}{ky} \right)^2 \right\} d\Omega;$$
$$\mathbf{f}_{\nu_1} = -\int_\Gamma \mathbf{N}^T \mathbf{N} n_i \{\hat{\nu} \mathbf{u_i}\} d\Gamma + \frac{1}{Re\sigma_{\tilde{\nu}}} \int_\Gamma \mathbf{N}^T \mathbf{N} n_i (1+\hat{\nu}) \left\{ \frac{\partial \hat{\nu}}{\partial \mathbf{x}_i} \right\} d\Gamma; \tag{A.3}$$
$$\mathbf{K}_{\nu_2} = -\int_\Omega \frac{\partial \mathbf{N}^T}{\partial \mathbf{x}_j} u_j \frac{\partial \mathbf{N}}{\partial \mathbf{x}_i} \{\hat{\nu} \mathbf{u_i}\} d\Omega - C_{b_1} \int_\Gamma \mathbf{N}^T n_j u_j \mathbf{N} \hat{\Omega} \{\hat{\nu}\} d\Gamma$$
$$-\frac{C_{w_1} f_w}{Re} \int_\Omega \frac{\partial \mathbf{N}^T}{\partial \mathbf{x}_j} u_j \mathbf{N} \left\{ \left(\frac{\hat{\nu}}{ky} \right)^2 \right\} d\Omega + \frac{C_{w_1} f_w}{Re} \int_\Gamma \mathbf{N}^T u_j \mathbf{N} \left\{ \left(\frac{\hat{\nu}}{ky} \right)^2 \right\} d\Gamma$$
$$\mathbf{f}_{\nu_2} = C_{b_1} \int_\Omega \frac{\partial \mathbf{N}^T}{\partial \mathbf{x}_j} u_j \mathbf{N} \hat{\Omega} \{\hat{\nu}\} d\Omega + \int_\Gamma \mathbf{N}^T \mathbf{N} n_j u_j \left\{ \frac{\partial (\hat{\nu} \mathbf{u_i})}{\partial \mathbf{x}_i} \right\} d\Gamma$$

Bibliography

[1] R C Allen, R A White, C K Zarins, and T J Fogarty. What are the characteristics of the ideal endovascular graft for abdominal aortic aneurysm exclusion? *Journal of endovascular surgery the official journal of the International Society for Endovascular Surgery*, 4(2):195–202, 1997.

[2] Frank R. Arko, Konstantinos A. Filis, Scott A. Seidel, Jim Gonzalez, Steve J. Lengle, Ron Webb, John Rhee, and Christopher K. Zarins. How many patients with infrarenal aneurysms are candidates for endovascular repair? the northern california experience. *Journal of Endovascular Therapy*, 11(1):33–40, February 2004.

[3] A. Athanasious, Kyriacos and M. Natoli, Roman. *Introduction to Continuum Biomechanics*, chapter Blood and Circulation, pages 123–138. Morgan and Claypool, 2008.

[4] Ali Azizzadeh, Luis A. Sanchez, Brian G. Rubin, Juan C. Parodi, Christopher J. Godshall, Patrick J. Geraghty, Eric T. Choi, M. Wayne Flye, John A. Curci, and Gregorio A. Sicard. Aortic neck attachment failure and the aneurx graft: Incidence, treatment options, and early results. *Annals of Vascular Surgery*, 19(4):516 – 521, 2005.

[5] Chris N. Bakoyiannis, Konstantinos P. Economopoulos, Sotirios Georgopoulos, Chris Klonaris, Maria Shialarou, Marina Kafeza, and Efstathios Papalambros. Fenestrated and branched endografts for the treatment of thoracoabdominal aortic aneurysms: A systematic review. *Journal of Endovascular Therapy*, 17(2):201–209, April 2010.

[6] Donald T. Baril, Ronald A. Kahn, Sharif H. Ellozy, Alfio Carroccio, and Michael L. Marin. Endovascular abdominal aortic aneurysm repair: Emerging developments and anesthetic considerations, October 2007.

[7] Peyman Benharash, Jason T. Lee, Oscar J. Abilez, Tami Crabtree, Daniel A. Bloch, and Christopher K. Zarins. Iliac fixation inhibits migration of both suprarenal and infrarenal aortic endografts, February 2007.

[8] R. L. T. Bevan, Igor Sazonov, Prihambodo H. Saksono, Perumal Nithiarasu, Raoul van Loon, Heyman Luckraz, and Saeed Ashraf. Patient-specific blood flow simulation through an aneurysmal thoracic aorta with a folded proximal neck. *International Journal for Numerical Methods in Biomedical Engineering*, 27(8):1167–1184, 2011.

[9] J. Blazek. *Computational Fluid Dynamics: Principles and Applications*, chapter Turbulence Modelling, page 241. Elsevier Science Ltd., 2001.

[10] Peter M. Brown, David T. Zelt, and Boris Sobolev. The risk of rupture in untreated aneurysms: The impact of size, gender, and expansion rate. *Journal of Vascular Surgery*, 37(2):280 – 284, 2003.

[11] J Brunkwall. How to design the optimal stent graft–what have we learnt? *Scandinavian journal of surgery SJS official organ for the Finnish Surgical Society and the Scandinavian Surgical Society*, 97(2):191–194, 2008.

[12] Piergiorgio Cao, Fabio Verzini, Gianbattista Parlani, Paola De Rango, Basso Parente, Giuseppe Giordano, Stefano Mosca, and Agostino Maselli. Predictive factors and clinical consequences of proximal aortic neck dilatation in 230 patients undergoing abdominal aorta aneurysm repair with self-expandable stent-grafts1 1 competition of interest: none., June 2003.

[13] Jeffrey P. Carpenter, Richard A. Baum, Clyde F. Barker, Michael A. Golden, Omaida C. Velazquez, Mark E. Mitchell, and Ronald M. Fairman. Durability of benefits of endovascular versus conventional abdominal aortic aneurysm repair. *Journal of Vascular Surgery*, 35(2):222 – 228, 2002.

[14] Tuncer Cebeci, Jian P. Shao, Fassi Kafyeke, and Eric Laurendeau. *Computational Fluid Dynamics for Engineers*, chapter Turbulence Models, page 87. Horizons Publishing Inc. and Springer Berlin Heidelberg, 2005.

[15] Emanuele Cecchi, Cristina Giglioli, Serafina Valente, Chiara Lazzeri, Gian Franco Gensini, Rosanna Abbate, and Lucia Mannini. Role of hemodynamic shear stress in cardiovascular disease. *Atherosclerosis*, 214(2):249 – 256, 2011.

[16] Jae-Sung Cho, Jang Yong Kim, Robert Y. Rhee, NavYash Gupta, Luke K. Marone, Ellen D. Dillavou, and Michel S. Makaroun. Contemporary results of open repair of ruptured abdominal aortoiliac aneurysms: Effect of surgeon volume on mortality. *Journal of Vascular Surgery*, 48(1):10 – 18, 2008.

[17] Eric T. Choi, Charles W. Wyble, Brian G. Rubin, Luis A. Sanchez, Robert W. Thompson, M.Wayne Flye, and Gregorio A. Sicard. Evolution of vascular fellowship training in the new era of endovascular techniques. *Journal of Vascular Surgery*, 33(2, Part B):106 – 110, 2001.

[18] E. Choke, G. Cockerill, W.R.W. Wilson, S. Sayed, J. Dawson, I. Loftus, and M.M. Thompson. A review of biological factors implicated in abdominal aortic aneurysm rupture. *European Journal of Vascular and Endovascular Surgery*, 30(3):227 – 244, 2005.

[19] Edward Choke, Graham Munneke, Robert Morgan, Anna-Maria Belli, Joseph Dawson, Ian Loftus, Robert McFarland, Thomas Loosemore, and Matthew Thompson. Visceral and renal artery complications of suprarenal fixation during endovascular aneurysm repair. *CardioVascular and Interventional Radiology*, 30:619–627, 2007. 10.1007/s00270-007-9008-7.

[20] Edward Choke, Graham Munneke, Robert Morgan, Anna-Maria Belli, Ian Loftus, Robert McFarland, Thomas Loosemore, and Matthew Thompson. Outcomes of endovascular abdominal aortic aneurysm repair in patients with hostile neck anatomy. *CardioVascular and Interventional Radiology*, 29:975–980, 2006. 10.1007/s00270-006-0011-1.

[21] Timothy A.M. Chuter. Branched and fenestrated stent grafts for endovascular repair of thoracic aortic aneurysms. *Journal of Vascular Surgery*, 43(2, Supplement):A111 – A115, 2006.

[22] W.Darrin Clouse, David C Brewster, Luke K Marone, Richard P Cambria, Glenn M LaMuraglia, Michael T Watkins, Christopher J Kwolek, Chieh-Min Fan, Stuart C Geller, and William M Abbott. Durability of aortouniiliac endografting with femorofemoral crossover: 4-year experience in the evt/guidant trials. *Journal of Vascular Surgery*, 37(6):1142 – 1149, 2003.

[23] Joseph S. Coselli, Suat Bket, and Bosco Djukanovic. Aortic arch operation: Current treatment and results. *The Annals of Thoracic Surgery*, 59(1):19 – 27, 1995.

[24] Colin M Crawford, Kristin Hurtgen-Grace, Ernest Talarico, and John Marley. Abdominal aortic aneurysm: an illustrated narrative review. *J Manipulative Physiol Ther*, 26(3):184–195, March 2003.

[25] Mital Desai, James Eaton-Evans, Claire Hillery, Raheleh Bakhshi, Zhong You, Jian Lu, George Hamilton, and Alexander Seifalian. Aaa stent grafts: Past problems and future prospects. *Annals of Biomedical Engineering*, 38:1259–1275, 2010. 10.1007/s10439-010-9953-1.

[26] Marcus J. Dill-Macky, Stephanie R. Wilson, Yarron Sternbach, John Kachura, and Thomas Lindsay. Detecting endoleaks in aortic endografts using contrast-enhanced sonography. *American Journal of Roentgenology*, 188(3):W262–W268, 2007.

[27] Ellen D Dillavou, Satish C Muluk, Robert Y Rhee, Edith Tzeng, Jonathan D Woody, Navyash Gupta, and Michel S Makaroun. Does hostile neck anatomy preclude successful endovascular aortic aneurysm repair? *Journal of Vascular Surgery*, 38(4):657 – 663, 2003.

[28] T.W. Duerig and M. Wholey. A comparison of balloon- and self-expanding stents. *Minimally Invasive Therapy & Allied Technologies*, 11(4):173–178, 2002.

[29] Jonathan Eliason and Gilbert Upchurch. Endovascular treatment of aortic aneurysms: State of the art. *Current Treatment Options in Cardiovascular Medicine*, 11:136–145, 2009. 10.1007/s11936-009-0014-8.

[30] Stephane Elkouri, Eugenio Martelli, Peter Gloviczki, Michael A. McKusick, Jean M. Panneton, James C. Andrews, Audra A. Noel, Thomas C. Bower, Timothy M. Sullivan, Charles Rowland, Tanya L. Hoskin, and Kenneth J. Cherry. Most patients with abdominal aortic aneurysm are not suitable for endovascular repair using currently approved bifurcated stent-grafts. *Vascular and Endovascular Surgery*, 38(5):401–412, September/October 2004.

[31] E. Erturk, T. C. Corke, and C. Gökçöl. Numerical solutions of 2-d steady incompressible driven cavity flow at high reynolds numbers. *International Journal for Numerical Methods in Fluids*, 48(7):747–774, 2005.

[32] Ercan Erturk. Nature of driven cavity flow at high-re and benchmark solutions on fine grid mesh.

[33] Mark Fillinger. Who should we operate on and how do we decide: Predicting rupture and survival in patients with aortic aneurysm. *Seminars in Vascular Surgery*, 20(2):121 – 127, 2007. ¡ce:title¿Changing Techniques in the Evaluation of Aortic Disease¡/ce:title¿ ¡xocs:full-name¿Changing Techniques in the Evaluation of Aortic Disease¡/xocs:full-name¿.

[34] Mark F. Fillinger, Steven P. Marra, M.L. Raghavan, and Francis E. Kennedy. Prediction of rupture risk in abdominal aortic aneurysm during observation: Wall stress versus diameter. *Journal of Vascular Surgery*, 37(4):724 – 732, 2003.

[35] Samuel R.G. Finlayson, John D. Birkmeyer, Mark F. Fillinger, and Jack L. Cronenwett. Should endovascular surgery lower the threshold for repair of abdominal aortic aneurysms? *Journal of Vascular Surgery*, 29(6):973 – 985, 1999.

[36] J. A. Fletcher, C. *Computational Techniques for Fluid Dynamics 1 Fundamental and General Techniques*, chapter Weighted Residual Method, page 116. Springer-Verlag, 2006.

[37] Thomas J. Fogarty, Frank R. Arko, and Christopher K. Zarins. Endograft technology: Highlights of the past 10 years. *Journal of Endovascular Therapy*, 11(SupplementII):II–192–II–199, December 2004.

[38] National Institute for Health and Clinical Excellence. Endovascular stent-grafts for the treatment of abdominal aortic aneurysm. NICE technology appraisal guidance 167, February 2009. Reviewed January 2012.

[39] Theofanis Fotis, Georgia Tsoumakidou, Theophanis Katostaras, Athina Kalokairinou, Evangelos Konstantinou, Vozides Kiki, and Theodosios Perdikides. Cost and effectiveness comparison of endovascular aneurysm repair versus open surgical repair of abdominal aortic aneurysm: A single-center experience. *Journal of Vascular Nursing*, 26(1):15 – 21, 2008.

[40] F. Bastos Goncalves, J.-P.P.M. de Vries, J.W. van Keulen, H. Dekker, F.L. Moll, J.A. van Herwaarden, and H.J.M. Verhagen. Severe proximal aneurysm neck angulation: Early results using the endurant stentgraft system. *European Journal of Vascular and Endovascular Surgery*, 41(2):193 – 200, 2011.

[41] William Grande and S. William Stavropoulos. Treatment of complications following endovascular repair of abdominal aortic aneurysms. *Semin intervent Radiol*, 23(02):156,164–, 2006.

[42] K. Greenberg, Roy. Endovascular aneurysm repair using branched or fenestrated devices. Clinical Case Studies in the Third Dimension Volume 1. Section 7: Vascular and Interventional Imaging; pp205-214.

[43] Roy K Greenberg. Abdominal aortic endografting:: Fixation and sealing. *Journal of the American College of Surgeons*, 194(1, Supplement 1):S79 – S87, 2002.

[44] Roy K. Greenberga, Michael Lawrence-Brownb, Guru Bhandaria, David Hartleyb, Wolf Stelterc, Tomas Umscheidc, Timothy Chuterd, Krassnador Ivanceve, Richard Greenf, Brian Hopkinsong, James Semmensh, and Ken Ouriela. An update of the zenith endovascular graft for abdominal aortic aneurysms: Initial implantation and mid-term follow-up data. *Journal of Vascular Surgery*, 33(2, Part B):157 – 164, 2001.

[45] RM Greenhalgh. Comparison of endovascular aneurysm repair with open repair in patients with abdominal aortic aneurysm (evar trial 1), 30-day operative mortality results: randomised controlled trial, September 2004.

[46] D.W. Harkin, M. Dillon, P.H. Blair, P.K. Ellis, and F. Kee. Endovascular ruptured abdominal aortic aneurysm repair (evrar): A systematic review. *European Journal of Vascular and Endovascular Surgery*, 34(6):673 – 681, 2007.

[47] Maarit A. Heikkinen, Jean Marc Alsac, Frank R. Arko, Riina Metsänoja, Agnis Zvaigzne, and Christopher K. Zarins. The importance of iliac fixation in prevention of stent graft migration. *Journal of Vascular Surgery*, 43(6):1130 – 1137, 2006.

[48] Maarit A. Heikkinen, Frank R. Arko, and Christopher K. Zarins. What is the significance of endoleaks and endotension, October 2004.

[49] Michael S. Heng, Michael J. Fagan, Jason W. Collier, Grishma Desai, Peter T. McCollum, and Ian C. Chetter. Peak wall stress measurement in elective and acute abdominal aortic aneurysms. *Journal of Vascular Surgery*, 47(1):17 – 22, 2008.

[50] R. Hinchliffe and K. Ivancev. Endovascular aneurysm repair: Current and future status. *CardioVascular and Interventional Radiology*, 31:451–459, 2008. 10.1007/s00270-008-9295-7.

[51] Roel Hobo, Jur Kievit, Lina J. Leurs, and Jacob Buth. Influence of severe infrarenal aortic neck angulation on complications at the proximal neck following endovascular aaa repair: A eurostar study. *Journal of Endovascular Therapy*, 14(1):1–11, February 2007.

[52] A D Jeays, P V Lawford, R Gillott, P Spencer, D C Barber, K D Bardhan, and D R Hose. Characterisation of the haemodynamics of the superior mesenteric artery. *Journal of Biomechanics*, 40(9):1916–1926, 2007.

[53] RAGHUNANDAN KAMINENI and RICHARD R. HEUSER. Abdominal aortic aneurysm:. *Journal of Interventional Cardiology*, 17(6):437–445, 2004.

[54] Kuribayashi Kaori. *A novel foldable stent graft.* PhD thesis, University of Oxford, Mathematical,Physical & Life Sciences Division - Engineering Science, 2004. Chapter:02 Page 10, 26.

[55] Demosthenes Katritsis, Lambros Kaiktsis, Andreas Chaniotis, John Pantos, Efstathios P. Efstathopoulos, and Vasilios Marmarelis. Wall shear stress: Theoretical considerations and methods of measurement. *Progress in Cardiovascular Diseases*, 49(5):307 – 329, 2007. ¡ce:title¿Special Articles¡/ce:title¿.

[56] John A. Kaufman, Stuart C. Geller, David C. Brewster, Chieh-Min Fan, Richard P. Cambria, Glenn M. LaMuraglia, Jonathan P. Gertler, William M. Abbott, and Arthur C. Waltman. Endovascular repair of abdominal aortic aneurysms. *American Journal of Roentgenology*, 175(2):289–302, 2000.

[57] Allen P. Klippel and Harvey R. Butcher Jr. The unoperated abdominal aortic aneurysm. *The American Journal of Surgery*, 111(5):629 – 631, 1966.

[58] Bas Koenen, F.N. van de Vosse, L. Speelman, M.C.M. Rutten, and C.C. van Donkelaar. Towards the design of a patient specific stentgraft for endovascular aortic repair. Graduation thesis, Eindhoven University of Technology, Netherlands, http://www.mate.tue.nl/mate/showabstract.php/7883, March 2007.

[59] David N. Ku. Blood flow in arteries. *Annual Review of Fluid Mechanics*, 29(1):399–434, 1997.

[60] D. Kwak, C. Kiris, and J. Dacles-Mariani. An assessment of artificial compressibility and pressure projection methods for incompressible flow simulations. In Charles-Henri Bruneau, editor, *Sixteenth International Conference on Numerical Methods in Fluid Dynamics*, volume 515 of *Lecture Notes in Physics*, pages 177–182. Springer Berlin / Heidelberg, 1998. 10.1007/BFb0106580.

[61] Dochan Kwak and Cetin C. Kiris. *Computation of viscous incompressible flows*, chapter Artificial Compressibility Method, pages 41–47. Springer, 2011.

[62] D. Laganá, G. Carrafiello, M. Mangini, A. Giorgianni, R. Caronno, P. Castelli, G. Dionigi, S. Cuffari, and C. Fugazzola. Management and endovascular treatment of symptomatic abdominal aortic aneurysms. *La Radiologia Medica*, 111:959–970, 2006. 10.1007/s11547-006-0094-4.

[63] Stephen Lalka, Matthew Johnson, Jan Namyslowski, Michael Dalsing, Dolores Cikrit, Alan Sawchuk, Shoaib Shafique, Ryan Nachreiner, and Elaine OBrien. Renal interventions after abdominal aortic aneurysm repair using an aortic endograft with suprarenal fixation. *The American Journal of Surgery*, 192(5):577 – 582, 2006. ¡ce:title¿PAPERS FROM THE ASSOCIATION OF VA SURGEONS¡/ce:title¿ ¡xocs:full-name¿30th Annual Meeting¡/xocs:full-name¿.

[64] Emma Larsson, Fausto Labruto, T. Christian Gasser, Jesper Swedenborg, and Rebecka Hultgren. Analysis of aortic wall stress and rupture risk in patients with abdominal aortic aneurysm with a gender perspective. *Journal of Vascular Surgery*, 54(2):295 – 299, 2011.

[65] L.Louis Lau, Albert G Hakaim, W.Andrew Oldenburg, Beate Neuhauser, J.Mark McKinney, Ricardo Paz-Fumagalli, and Andrew Stockland. Effect of suprarenal versus infrarenal aortic endograft fixation on renal function and renal artery patency: a comparative study with intermediate follow-up. *Journal of Vascular Surgery*, 37(6):1162 – 1168, 2003.

[66] Frank A. Lederle, Gary R. Johnson, and Samuel E. Wilson. Abdominal aortic aneurysm in women. *Journal of Vascular Surgery*, 34(1):122 – 126, 2001.

[67] Roman A. Litwinski, Carlos E. Donayre, Sheryl L. Chow, Tae K. Song, George Kopchok, Irwin Walot, and Rodney A. White. The role of aortic neck dilation and elongation in the etiology of stent graft migration after endovascular abdominal aortic aneurysm repair with a passive fixation device, December 2006.

[68] M. Malina, J. Brunkwall, K. Ivancev, M. Lindh, B. Lindblad, and B. Risberg. Renal arteries covered by aortic stents: Clinical experience from endovascular grafting of aortic aneurysms, August 1997.

[69] Carlos Henrique Marchi, Roberta Suero, and Luciano Kiyoshi Araki. The lid-driven square cavity flow: numerical solution with a 1024 x 1024 grid. *Journal of the Brazilian Society of Mechanical Sciences and Engineering*, 31:186 – 198, 09 2009.

[70] Michael L. Marin, Larry H. Hollier, Sharif H. Ellozy, David Spielvogel, Harold Mitty, Randall Griepp, Robert A. Lookstein, Alfio Carroccio, Nicholas J. Morrissey, Victoria J. Teodorescu, Tikva S. Jacobs, Michael E. Minor, Claudie M. Sheahan, Kristina Chae, Juliana Oak, and Andrew Cha. Endovascular stent graft repair of abdominal and thoracic aortic aneurysms: A ten-year experience with 817 patients. *Annals of Surgery*, 238(4):–, 2003.

[71] N. Massarotti, P. Nithiarasu, and O. C. Zienkiewicz. Characteristic-based-split (CBS) algorithm for incompressible flow problems with heat transfer. *International Journal of Numerical Methods for Heat & Fluid Flow*, Volume 8:pp.969 – 990, 1998.

[72] Tara M. Mastracci, Luis Garrido-Olivares, Claudio S. Cin, and Catherine M. Clase. Endovascular repair of ruptured abdominal aortic aneurysms: A systematic review and meta-analysis. *Journal of Vascular Surgery*, 47(1):214 – 221.e14, 2008.

[73] James McPhee, Mohammad H Eslami, Elias J Arous, Louis M Messina, and Andres Schanzer. Endovascular treatment of ruptured abdominal aortic aneurysms in the united states (2001-2006): a significant survival benefit over open repair is independently associated with increased institutional volume. *Journal of vascular surgery official publication the Society for Vascular Surgery and International Society for Cardiovascular Surgery North American Chapter*, 49(4):817–826, 2009.

[74] A. Millon, A. Deelchand, P. Feugier, J.M. Chevalier, and J.P. Favre. Conversion to open repair after endovascular aneurysm repair: Causes and results. a french multicentric study. *European Journal of Vascular and Endovascular Surgery*, 38(4):429 – 434, 2009.

[75] S Molony, David, Anthony Callanan, G Kavanagh, Eamon, T Walsh, Michael, and M McGloughlin, Tim. Fluid-structure interaction of a patient-specific abdominal aortic aneurysm treated with an endovascular stent-graft. *BioMedical Engineering OnLine*, 8, 2009.

[76] W.S. Moore. The role of endovascular grafting technique in the treatment of infrarenal abdominal aortic aneurysm. *Cardiovascular Surgery*, 3(2):109 – 114, 1995.

[77] Konstantinos G. Moulakakis, Ilias Dalainas, Spyridon Mylonas, Triantafillos G. Giannakopoulos, Efthimios D. Avgerinos, and Christos D. Liapis. Conversion to open repair after endografting for abdominal aortic aneurysm: A review of causes, incidence, results, and surgical techniques of reconstruction. *Journal of Endovascular Therapy*, 17(6):694–702, December 2010.

[78] Bart E. Muhs, Eric L.G. Verhoeven, Clark J. Zeebregts, Ignace F.J. Tielliu, Ted R. Prins, Hence J.M. Verhagen, and Jan J.A.M. van den Dungen. Mid-term results of endovascular aneurysm repair with branched and fenestrated endografts. *Journal of Vascular Surgery*, 44(1):9 – 15, 2006.

[79] Hans O. Myhre, Jan Lundbom, and Staal Hatlinghus. Endovascular treatment of aortic disease. *International Journal of Angiology*, 9:10–17, 2000. 10.1007/BF01616322.

[80] Tony Nicholson. Endovascular stent grafting of abdominal aortic aneurysms a radiologist's view on a new potential issue in renovascular disease. *Journal of Renovascular Disease*, 2:pp 34–36, June 2003.

[81] Westerhof Nico, Stergiopulos Nikos, and Noble Mark, I.M. *Snapshots of Hemodynamics An aid for clinical research and Graduate education*, chapter Viscosity and law of poiseuille, pages 3–8. Springer Science and Business Media, Inc., 2005.

[82] P. Nithiarasu. An efficient artificial compressibility (ac) scheme based on the characteristic based split (cbs) method for incompressible flows. *International Journal for Numerical Methods in Engineering*, 56(13):1815–1845, 2003.

[83] Theodore G. Papaioannou, Emmanouil N. Karatzis, Manolis Vavuranakis, John P. Lekakis, and Christodoulos Stefanadis. Assessment of vascular wall shear stress and implications for atherosclerotic disease. *International Journal of Cardiology*, 113(1):12 – 18, 2006.

[84] Shane S. Parmer and Jeffrey P. Carpenter. Endovascular aneurysm repair with suprarenal vs infrarenal fixation: A study of renal effects. *Journal of Vascular Surgery*, 43(1):19 – 19.e9, 2006.

[85] Juan Carlos Parodi. Endovascular repair of abdominal aortic aneurysms and other arterial lesions. *Journal of Vascular Surgery*, 21(4):549 – 557, 1995.

[86] Sheela T. Patel, Paul B. Haser, Harry L. Bush Jr, and K.Craig Kent. The cost-effectiveness of endovascular repair versus open surgical repair of abdominal aortic aneurysms: A decision analysis model. *Journal of Vascular Surgery*, 29(6):958 – 972, 1999.

[87] Noud Peppelenbosch, Jacob Buth, Peter L. Harris, Corine van Marrewijk, and Gerdine Fransen. Diameter of abdominal aortic aneurysm and outcome of endovascular aneurysm repair: does size matter? a report from eurostar. *Journal of Vascular Surgery*, 39(2):288 – 297, 2004.

[88] Mario J. Perko, Martin Nrgaard, Tina M. Herzog, Peter Skov Olsen, Torben V. Schroeder, and Gsta Pettersson. Unoperated aortic aneurysm: A survey of 170 patients. *The Annals of Thoracic Surgery*, 59(5):1204 – 1209, 1995.

[89] David Pintoux, Philippe Chaillou, Laure Azema, Philippe Bizouarn, Alain Costargent, Philippe Patra, and Yann Gouffic. Long-term influence of suprarenal or infrarenal fixation on proximal neck dilatation and stentgraft migration after evar. *Annals of Vascular Surgery*, 25(8):1012 – 1019, 2011.

[90] Pranowo and Gatot Bintoro. Artificial compressibility method for steady circulation flow in the lid driven cavity. Presented in the International Seminar on Numerical Analysis in Engineering (NAE), March 2000.

[91] Monique Prinssen, Christopher L. Wixon, Erik Buskens, and Jan D. Blankensteijn. Surveillance after endovascular aneurysm repair: Diagnostics, complications, and associated costs. *Annals of Vascular Surgery*, 18(4):421 – 427, 2004.

[92] Robert S. Reneman, Hans Vink, and Arnold P.G. Hoeks. Wall shear stress revisited. *Artery Research*, 3(2):73 – 78, 2009.

[93] T Resch, M Malina, B Lindblad, J Malina, J Brunkwall, and K Ivancev. The impact of stent design on proximal stent-graft fixation in the abdominal aorta: an experimental study. *European Journal of Vascular and Endovascular Surgery*, 20(2):190 – 195, 2000.

[94] Joseph J. Ricotta and Gustavo S. Oderich. Fenestrated and branched stent grafts. *Perspectives in Vascular Surgery and Endovascular Therapy*, 20(2):174–187, 2008.

[95] Robert B. Rutherford. Endovascular aneurysm repair and outcome in patients unfit for open repair of abdominal aortic aneurysm (evar trial 2): Randomized controlled trial. *Perspectives in Vascular Surgery and Endovascular Therapy*, 18(1):76–77, 2006.

[96] Umar Sadat, Jonathan R. Boyle, Stewart R. Walsh, Tjun Tang, Kevin Varty, and Paul D. Hayes. Endovascular vs open repair of acute abdominal aortic aneurysmsa systematic review and meta-analysis, July 2008.

[97] Srgio M. Sampaio, Jean M. Panneton, Geza I. Mozes, James C. Andrews, Thomas C. Bower, Manju Kalra, Kenneth J. Cherry, Timothy Sullivan, and Peter Gloviczki. Aneurysm sac thrombus load predicts type ii endoleaks after endovascular aneurysm repair. *Annals of Vascular Surgery*, 19(3):302 – 309, 2005.

[98] Giuseppe Sangiorgi, Gloria Melzi, Pierfrancesco Agostoni, Clarissa Cola, Fabrizio Clementi, Paolo Romitelli, Renu Virmani, and Antonio Colombo. Engineering aspects of stents design and their translation into clinical practice. *Annali dellÍstituto superiore di sanitá ISSN 0021-2571*, 43(1):89–100, 2007.

[99] Igor Sazonov, Si Yong Yeo, Rhodri L. T. Bevan, Xianghua Xie, Raoul van Loon, and Perumal Nithiarasu. Modelling pipeline for subject-specific arterial blood flow "A review". *International Journal for Numerical Methods in Biomedical Engineering*, 27(12):1868–1910, 2011.

[100] C. Scanlon, Valerie and Sanders Tina. *Essentials of anatomy and physiology*, chapter The Heart, pages 278, 283. F. A. Davis Company, 2007.

[101] Marc L. Schermerhorn, Kristina A. Giles, Allen D. Hamdan, Suzanne E. Dalhberg, Robert Hagberg, and Frank Pomposelli. Population-based outcomes of open descending thoracic aortic aneurysm repair. *Journal of Vascular Surgery*, 48(4):821 – 827, 2008.

[102] Seeley, Stephens, and Tate. *Anatomy and Physiology, Sixth Edition*, chapter Cardiovascular System, The Heart, pages 686, 688. The McGraw Hill Companies, 2004.

[103] Akram M. Shaaban and Andr J. Duerinckx. Wall shear stress and early atherosclerosis. *American Journal of Roentgenology*, 174(6):1657–1665, 2000.

[104] N Shahcheraghi, HA Dwyer, AY Cheer, AI Barakat, and T. Rutaganira. Unsteady and three-dimensional simulation of blood flow in the human aortic arch. *J Biomech Eng.*, 124(4):378–87., 2002 Aug;.

[105] L Shedden, K Oldroyd, and P Connolly. Current issues in coronary stent technology. *Proceedings of the Institution of Mechanical Engineers, Part H: Journal of Engineering in Medicine*, 223(5):515–524, 2009.

[106] Harry A Silber, David A Bluemke, Pamela Ouyang, Yiping P Du, Wendy S Post, and Joao A.C Lima. The relationship between vascular wall shear stress and flow-mediated dilation: endothelial function assessed by phase-contrast magnetic resonance angiography. *Journal of the American College of Cardiology*, 38(7):1859 – 1865, 2001.

[107] Benjamin W. Starnes, Elina Quiroga, Carolyn Hutter, Nam T. Tran, Thomas Hatsukami, Mark Meissner, Gale Tang, and Ted Kohler. Management of ruptured abdominal aortic aneurysm in the endovascular era. *Journal of Vascular Surgery*, 51(1):9 – 18, 2010.

[108] PD Stein and HN Sabbah. Turbulent blood flow in the ascending aorta of humans with normal and diseased aortic valves. *Circulation Research*, 39(1):58–65, 1976.

[109] W.Charles Sternbergh, Glen Carter, John W. York, Moises Yoselevitz, and Samuel R. Money. Aortic neck angulation predicts adverse outcome with endovascular abdominal aortic aneurysm repair, March 2002.

[110] David H. Stone, David C. Brewster, Christopher J. Kwolek, Glenn M. LaMuraglia, Mark F. Conrad, Thomas K. Chung, and Richard P. Cambria. Stent-graft versus open-surgical repair of the thoracic aorta: Mid-term results. *Journal of Vascular Surgery*, 44(6):1188 – 1197, 2006.

[111] Pavel V. Stroev, Peter R. Hoskins, and William J. Easson. Distribution of wall shear rate throughout the arterial tree: A case study. *Atherosclerosis*, 191(2):276 – 280, 2007.

[112] Zhonghua Sun, Thanapong Chaichana, Manas Sangworasil, and Supan Tungjitkusolmun. Computational fluid analysis of blood flow characteristics in abdominal aortic aneurysms treated with suprarenal endovascular grafts. In Chwee Teck Lim, James C. H. Goh, and Ratko Magjarevic, editors, *13th International Conference on Biomedical Engineering*, volume 23 of *IFMBE Proceedings*, pages 1728–1732. Springer Berlin Heidelberg, 2009. 10.1007/978-3-540-92841-6_429.

[113] Andrew L. Tambyraja, Simon C.A. Fraser, John A. Murie, and Roderick T.A. Chalmers. Functional outcome after open repair of ruptured abdominal aortic aneurysm. *Journal of Vascular Surgery*, 41(5):758 – 761, 2005.

[114] Bernard W. Thompson, Gary Meek, and Masauki Hara. Resection of abdominal aortic aneurysms. *The American Journal of Surgery*, 116(5):682 – 685, 1968. ¡ce:title¿Papers of the Southwestern Surgical Congress¡/ce:title¿.

[115] Matt Thompson. Infrarenal abdominal aortic aneurysms. *Current Treatment Options in Cardiovascular Medicine*, 5:137–146, 2003. 10.1007/s11936-003-0022-z.

[116] Britt H. Tonnessen, W. Charles Sternbergh III, and Samuel R. Money. Mid- and long-term device migration after endovascular abdominal aortic aneurysm repair: A comparison of aneurx and zenith endografts. *Journal of Vascular Surgery*, 42(3):392 – 401, 2005.

[117] Jonathan B. Towne. Endovascular treatment of abdominal aortic aneurysms, February 2005.

[118] HH Trout and HM Tanner. A new vascular endostaple: A technical description. *Journal of Vascular Surgery*, 34(3):565 – 568, 2001.

[119] S.Rao Vallabhaneni and P.L Harris. Lessons learnt from the eurostar registry on endovascular repair of abdominal aortic aneurysm repair. *European Journal of Radiology*, 39(1):34 – 41, 2001.

[120] M. Creemers E. Limet R. Van Damme, H. Deprez. Intrinsic structural failure of polyester (dacron) vascular grafts. a general review. *ACTA CHIRURGICA BELGICA*, VOl 105; NUMB 3:pages 249–255, May-June 2005. Publisher: AMB ACTA MEDICA BELGICA.

[121] J.W. van Keulen, J. van Prehn, M. Prokop, F.L. Moll, and J.A. van Herwaarden. Dynamics of the aorta before and after endovascular aneurysm repair: A systematic review. *European Journal of Vascular and Endovascular Surgery*, 38(5):586 – 596, 2009.

[122] Frank J. Veith, Michael L. Marin, Jacob Cynamon, Claudio Schonholz, and Juan Parodi. 1992: Parodi, montefiore, and the first abdominal aortic aneurysm stent graft in the united states, September 2005.

[123] Bart A.N. Verhoeven, Evert J. Waasdorp, Madhu L. Gorrepati, Joost A. van Herwaarden, Jan Albert Vos, Jan Wille, Frans L. Moll, Christopher K. Zarins, and Jean Paul P.M. de Vries. Long-term results of talent endografts for endovascular abdominal aortic aneurysm repair. *Journal of Vascular Surgery*, 53(2):293 – 298, 2011.

[124] Eric L. Verhoeven, Marten R. Kapma, Henk Groen, Ignace F. Tielliu, Clark J. Zeebregts, Foppe Bekkema, and Jan J. van den Dungen. Mortality of ruptured abdominal aortic aneurysm treated with open or endovascular repair. *Journal of Vascular Surgery*, 48(6):1396 – 1400, 2008.

[125] L. G. Verhoeven, E., F. J. Tielliu, I., E. Muhs, B., T. G. J. Bos, W., J. Zeebregts, C., R. Prins, T., I. Oranen B., and J. A. M. van den Dungen, J. Fenestrated and branched stent-grafting : a 5-years experience. *Acta Chirurgica Belgica*, 106:317–322, 2006.

[126] K Versteeg, H and W Malalasekera. *An introduction to computational fluid Mechanics*, chapter Turbulence and its modelling, pages 66, 89. Pearson Education Limited, Second Edition, 2007.

[127] Jacob J. Visser, Johanna L. Bosch, M.G. Myriam Hunink, Lukas C. van Dijk, Johanna M. Hendriks, Don Poldermans, and Marc R.H.M. van Sambeek. Endovascular repair versus open surgery in patients with ruptured abdominal aortic aneurysms: Clinical outcomes with 1-year follow-up. *Journal of Vascular Surgery*, 44(6):1148 – 1155, 2006.

[128] E.J. Waasdorp, J.-P.P.M. de Vries, A. Sterkenburg, J.-A. Vos, H.J.C. Kelder, F.L. Moll, and C.K. Zarins. The association between iliac fixation and proximal stent-graft migration during evar follow-up: Mid-term results of 154 talent devices. *European Journal of Vascular and Endovascular Surgery*, 37(6):681 – 687, 2009.

[129] Evert Waasdorp, Casper van't Hullenaar, Joost van Herwaarden, Hans Kelder, Eric van de Pavoordt, Tim Overtoom, Frans Moll, and Jean-Paul de Vries. Renal function after endovascular aortic aneurysm repair: A single-center experience with transrenal versus infrarenal fixation. *Journal of Endovascular Therapy*, 14(2):130–137, April 2007.

[130] Carl Magnus Wahlgren and Jonas Malmstedt. Outcomes of endovascular abdominal aortic aneurysm repair compared with open surgical repair in high-risk patients: Results from the swedish vascular registry. *Journal of Vascular Surgery*, 48(6):1382 – 1388, 2008.

[131] Reese A. Wain, Michael L. Marin, Takao Ohki, Luis A. Sanchez, Ross T. Lyon, Alla Rozenblit, William D. Suggs, John G. Yuan, and Frank J. Veith. Endoleaks after endovascular graft treatment of aortic aneurysms: Classification, risk factors, and outcome. *Journal of Vascular Surgery*, 27(1):69 – 80, 1998.

[132] Lee Waite and Jerry Fine. *Applied Biofluid Mechanics*, chapter Hematology and Blood Rheology, pages 111–116, 136, 202–210. McGraw-Hill Companies, 2007.

[133] Grace J. Wang and Jeffrey P. Carpenter. The powerlink system for endovascular abdominal aortic aneurysm repair: Six-year results. *Journal of Vascular Surgery*, 48(3):535 – 545.e3, 2008.

[134] Jolanda J. Wentzel, Frank J.H. Gijsen, Nikos Stergiopulos, Patrick W. Serruys, Cornelis J. Slager, and Rob Krams. Shear stress, vascular remodeling and neointimal formation. *Journal of Biomechanics*, 36(5):681 – 688, 2003. ¡ce:title¿Cardiovascular Biomechanics¡/ce:title¿.

[135] Geoffrey H. White. What are the causes of endotension? *Journal of Endovascular Therapy*, 8(5):454–456, October 2001.

[136] Geoffrey H. White, Weiyun Yu, James May, Xavier Chaufour, and Michael S. Stephen. Endoleak as a complication of endoluminal grafting of abdominal aortic aneurysms: Classification, incidence, diagnosis,and management. *Journal of Endovascular Surgery*, 4(2):152–168, May 1997.

[137] Jong Yun Won, Sang-Hyun Suh, Heung-kyu Ko, Kwang Hoon Lee, Won Heum Shim, Byung-Chul Chang, Dong Hoon Choi, Sang Joon Park, and Do Yun Lee. Problems encountered during and after stent-graft treatment of aortic dissection, February 2006.

[138] Li Xikui and Wu Wenhua. Characteristic galerkin method for convection-diffusion equations and implicit algorithm using precise integration. *Acta Mechanica Sinica*, 15:371–382, 1999. 10.1007/BF02487935.

[139] D Yoshino and K Inoue. Design method of self-expanding stents suitable for the patient's condition. *Proceedings of the Institution of Mechanical Engineers, Part H: Journal of Engineering in Medicine*, 224(9):1019–1038, 2010.

[140] S.W. Yusuf, S.C. Whitaker, T.A.M. Chuter, P.W. Wenham, and B.R. Hopkinson. Emergency endovascular repair of leaking aortic aneurysm. *The Lancet*, 344(8937):1645 –, 1994. ¡ce:title¿Originally published as Volume 2, Issue 8937¡/ce:title¿.

[141] Christopher K Zarins, Daniel A Bloch, Tami Crabtree, Alan H Matsumoto, Rodney A White, and Thomas J Fogarty. Stent graft migration after endovascular aneurysm repair: importance of proximal fixation. *Journal of Vascular Surgery*, 38(6):1264 – 1272, 2003.

[142] Christopher K. Zarins, Tami Crabtree, Daniel A. Bloch, Frank R. Arko, Kenneth Ouriel, and Rodney A. White. Endovascular aneurysm repair at 5 years: does aneurysm diameter predict outcome? *Journal of Vascular Surgery*, 44(5):920 – 930, 2006.

[143] CK Zarins, DP Giddens, BK Bharadvaj, VS Sottiurai, RF Mabon, and S Glagov. Carotid bifurcation atherosclerosis. quantitative correlation of plaque localization with flow velocity profiles and wall shear stress. *Circulation Research*, 53(4):502–514, 1983.

[144] C. Zeinkiewicz, O. and L. Taylor, R. *The Finite Element Method, Volume 3, FLUID DYNAMICS*, chapter Convection dominated problems–Finite element approximations to the convection-diffusion equations, pages 35–41. Butterworth-Heinemann, 2000.

[145] C. Zienkiewicz, O., L. Taylor, R., and P. Nithiarasu. *The Finite Element Method for Fluid Dynamics, sixth edition*, chapter Turbulent flows, pages 93, 251–256. Butterworth-Heinemann, 2005.